Comparison of terrestrial evapotranspiration estimates using the mass transfer and Penman-Monteith equations in land surface models

Jing Chen,[1] Baozhang Chen,[1] T. Andrew Black,[2] John L. Innes,[3] Guangyu Wang,[3] Gerard Kiely,[4] Takashi Hirano,[5] and Georg Wohlfahrt[6]

Received 15 July 2013; revised 18 October 2013; accepted 26 October 2013; published 13 December 2013.

[1] The mass transfer (MT) equation and the Penman-Monteith (PM) equation are two common approaches used in various land surface models for simulating evapotranspiration (ET). Yet assessments are rarely conducted to determine how well these structurally differing equations simulate ET across various biomes and climatic environments with different canopy upscaling strategies. We evaluated the capacity of models to estimate ET using the MT equation with the one-leaf strategy in the Community Land Model version 4 and the PM equation in the Dynamic Land Model using the one-leaf and two-leaf upscaling approaches for 22 selected eddy covariance flux towers representing 10 typical plant functional types. Overall, across half-hourly, daily, monthly, and seasonal scales, the MT equation performed less robust than the PM equation in forests. The former had 8–15% higher root-mean-square error and 1–4% lower index of agreement and a large uncertainty in warm and wet seasons for several sites. It leaves a doubt about its application of estimating ET across regional to global scales. Considering the net radiation available on the surface of leaf/soil and adopting the two-leaf approach made the PM equation closer to the EC measurements on average but still could not capture the variation during the cold season. We suggest that further improvements in simulation of ET require seasonal variation of some key parameters and quantification of spatial heterogeneity.

Citation: Chen, J., B. Chen, T. A. Black, J. L. Innes, G. Wang, G. Kiely, T. Hirano, and G. Wohlfahrt (2013), Comparison of terrestrial evapotranspiration estimates using the mass transfer and Penman-Monteith equations in land surface models, *J. Geophys. Res. Biogeosci.*, *118*, 1715–1731, doi:10.1002/2013JG002446.

1. Introduction

[2] Evapotranspiration (ET), which includes transpiration and evaporation from the soil-plant system, is a major component of the terrestrial water cycle and energy balance (i.e., latent heat flux, *LE*) [*Katul et al*., 2012]. This process returns ~ 60% of annual land precipitation to the atmosphere [*Jung et al*., 2010; *Oki and Kanae*, 2006], which affects and then is affected by local climate. One of the extensive adoptions for evaluating and predicting ET is the land surface models (LSMs) [*Jaksa et al*., 2013; *Vinukollu et al*., 2012]. Not only because LSMs have a mechanism-based structure and applicability to a wide range of space and time scales [*Chen and Coops*, 2009] but also it can be coupled to a global circulation model for estimating the effects of climate change and accounting for possible feedback [*Cox et al*., 2000; *Gent et al*., 2011; *Subin et al*., 2011]. Therefore, estimating ET and quantifying the process accurately in LSMs are critical to evaluating the potential impacts on the terrestrial water balance and climate change [*Bonan*, 2008; *Cao et al*., 2010].

[3] ET is estimated by meteorological data in models. The mass transfer (MT) equation is one of the classical methods to estimate terrestrial water vapor flux, based on the proportional relationship between vapor flux and vapor pressure difference [*Singh and Xu*, 1997; *Verstraeten et al*., 2008]. Based on the combination of mass and heat transfer equations, and the energy balance equation, many expressions have been derived, such as the Penman-Monteith (PM) equation [*Monteith*, 1965] and the Shuttleworth-Wallace equation [*Shuttleworth and Wallace*, 1985]. Much effort has been made to compare performances of different approaches to

Additional supporting information may be found in the online version of this article.

[1]State key Laboratory of Resources and Environmental Information System, Institute of Geographic Sciences and Nature Resources Research, Chinese Academy of Sciences, Beijing, China.
[2]Faculty of Land and Food Systems, University of British Columbia, Vancouver, British Columbia, Canada.
[3]Department of Forest Resources Management, University of British Columbia, Vancouver, British Columbia, Canada.
[4]Civil and Environmental Engineering Department, Environmental Research Institute, University College Cork, Cork, Ireland.
[5]Division of Environmental Resources, Research Faculty of Agriculture, Hokkaido University, Sapporo, Japan.
[6]Institute of Ecology, University of Innsbruck, Innsbruck, Austria.

Corresponding author: B. Chen, State key Laboratory of Resources and Environmental Information System, Institute of Geographic Sciences and Nature Resources Research, Chinese Academy of Sciences, Beijing, China. (Baozhang.chen@igsnrr.ac.cn)

2169-8953/13/10.1002/2013JG002446

ET estimation that is systematically independent from the land surface modeling systems [*Fisher et al*., 2005; *Nazeer*, 2010; *Sentelhas et al*., 2010; *Stannard*, 1993; *Tabari et al*., 2011; *Vinukollu et al*., 2011]. These studies paid considerable attention to selecting an ET equation which has a simple structure and an acceptable result, since some driven data are incomplete or unavailable [*Fisher et al*., 2005; *Nazeer*, 2010; *Sentelhas et al*., 2010; *Tabari et al*., 2011]. It has been shown that the uncertainties in ET estimation mainly stemmed from the differences of model structures [*Fisher et al*., 2005; *Tabari et al*., 2011].

[4] LSMs calculate the total water vapor flux with three parts: transpiration from the canopy, evaporation from the intercepted water by canopy, and evaporation from soil surface, in which the soil evaporation integrates with the soil moistures [*Chen et al*., 2007a; *Lawrence et al*., 2007]. Many LSMs adopt the MT equation to computer ET, such as the Community Land Surface Model (CLM) [*Oleson et al*., 2010], *ecosys* [*Grant et al*., 2012], and Cross-Chain Loran Atmospheric Sounding System [*Verseghy et al*., 1993]. CLM is the land surface model component of the Community Earth System Model (CESM, http://www2.cesm.ucar.edu/) developed by the National Center for Atmospheric Research (NCAR). The model uses an improved MT equation for determining transpiration and evaporation with the one-leaf upscaling strategy [*Oleson et al*., 2010]. Recent assessments of CLM version 4 indicated that the model can capture the spatial distribution and the interannual variability of ET well compared with observations-based estimates at a global scale [*Shi et al*., 2013]. The ET estimation has a better performance with improved model structure or/and parameters of plant canopy [*Bonan et al*., 2011]. *Bonan et al*. [2012] also reported that the modeled latent heat flux decreased in the tropics after replacing the two-leaf photosynthesis simulation method with a multilayer upscaling strategy. The PM equation is another option adopted by LSMs [*Chen et al*., 2007a; *Alton*, 2011]. One of them is the remote-sensing-based Ecosystem-Atmosphere Simulation Scheme (EASS) [*Chen et al*., 2007a]. EASS adopts the PM equation for modeling ET components and follows the sunlit-shaded leaf stratification strategy in both canopy-level photosynthesis and energy flux estimations. This canopy strategy enhanced the realism and accuracy in the simulation of net radiation and energy component fluxes of about 10% compared with the one-leaf strategy [*Chen et al*., 2007a]. In a further development, the EASS was coupled with the atmospheric global environmental multiscale model (GEM), and the EASS-GEM was reasonably successful in capturing both the spatial and temporal variation in energy fluxes [*Chen et al*., 2007b]. However, most of these results did not address the impact of the ET equation itself on the ET simulation or could not be used to improve the accuracy of estimation based on the functional structures.

[5] More than functional structures, less attention has been given to the model's suitability of water vapor flux for multiple biome types across different time scales and over relatively long time periods. Previous studies have only evaluated the ET (or *LE*) estimation performance of LSMs for individual sites [*Chen et al*., 2007a; *Grant et al*., 2005; *Wang et al*., 2011] or for a limited number of vegetation functional types [*Hou et al*., 2012; *Stöckli et al*., 2008], although lots of model-data comparison for many sites have been conducted in evaluating carbon dynamics models [*Keenan et al*., 2012; *Schaefer et al*., 2012; *Schwalm et al*., 2010; *Sprintsin et al*., 2012]. Another fact is that few existing performances of ET estimation operate across a number of time scales (diurnal to interannual). This would leave a debate about the success of ET simulation yearly. The issues mentioned above need to be clarified and resolved in order to reduce uncertainties in ET estimates at regional or global scales.

[6] In this study, we sought to address and to compare the performances of the MT equation in CLM and the PM equation in the Dynamic Land Model (DLM) using measurements of water vapor fluxes with the eddy covariance (EC) technique at typical sites for major biomes. DLM is an updated version of EASS. The selected EC towers represent 10 plant functional types across six biomes in three main climate zones. We tested the equations' ability at a series of time scales, including half-hourly, daily, monthly, and seasonal time scales, and then conducted a sensitivity test, so as to find the uncertainties in performance of these two equations for their potentials at regional or global scales. By using existing data set and uncertainty quantification, this research proves a solid foundation for evaluating equations to estimate water vapor flux in LSMs across multiple plant functional types and across a range of time scales.

2. Methods and Materials

2.1. FLUXNET Data

[7] We used the FLUXNET database (http://fluxnet.ornl.gov/) to calibrate the DLM and validate the water vapor flux estimates for both LSMs. The data set contains annual files of half-hourly flux and meteorological data at more than 400 EC stations across Europe (CarboEurope), America (AmeriFlux and Fluxnet-Canada), Asia (AisaFlux and ChinaFLUX), *etc*. We selected the EC towers according to a criterion in order to reduce the error derived from the observations by doing the following steps: (1) the site provides three or more years of continuous driver and validation data as a part of publicly accessible standardized level 4 or 3 database; (2) a "site-year" is accepted for analysis if more than 90% of the half hours in a year contained nonmissing values for each of the meteorological data (downwelling solar radiation, precipitation, wind speed, air temperature, and relative humidity) and the energy fluxes (net radiation (R_n), ground heat flux (G), latent heat flux (LE), and sensible heat flux *(H)*); and (3) energy balance closure is evaluated for each site-year according to the ratio of the dependent flux variables ($H + LE$) against the independently derived available energy ($R_n - G$) for each half hour [*Wilson et al*., 2002]. The values of the half-hourly energy balance closure ratio $(H + LE)/(R_n - G)$ deviated from the ideal closure (the value of 1) since random error exists [*Wilson et al*., 2002], so we recorded the number of the ratio within 0.6–1.4 in the daytime and then accepted a "site-year" when the accumulated number exceeded 60% of the total numbers of the half hour during the daytime of the growing season. Finally, 256 site-years were selected, representing eight biome types across three main climatic environments (i.e., plant functional types (PFTs)) [*Oleson et al*., 2010] at 67 EC sites. We used half of the sites for calibrating the model and used the others for the validation. Before that, energy fluxes were corrected for lack of energy balance closure by partitioning the available

Table 1. The Descriptions of Study Sites

Number	Site ID[a]	Latitude	Longitude	Elevation	Biome Type[b]	Climate Zone	Site-Year	Percipitation	Growing Season Length	LAImax	Soil Texture		References
											Sand (%)	Clay (%)	
1	CA-Ca1	49.867	−125.334	313	NEF	Temperate	2006	1456	253	7.3	81.4	3.7[f]	*Chen et al.* [2011a]; *Krishnan et al.* [2009]
2	DE-Tha	50.964	13.567	380	NEF	Temperate	1999	804	255	7.6	14.0	18.7	*Grünwald and Bernhofer* [2007]
3	ES-ES1	39.346	−0.319	1	NEF	Mediterranean	2005	414	317	2.6	72.4	0.3[g]	*Blyth et al.* [2010]
4	US-Ho1	45.204	−68.740	72	NEF	Temperate	2003	951	191	5.7	50.3	15.9	*Hollinger et al.* [2004]
5	CN-Qia	26.741	115.058	86	NEF	Temperate	2004	1325	-[d]	4.7	69.6	12.5	*Li et al.* [2007]
6	CA-Ojp	53.916	−104.692	518	NEF	Boreal	2008	418	147	2.0	32.9	27.7[f]	*Bergeron et al.* [2007]; *Kljun et al.* [2006]
7	CA-NS1	55.879	−98.484	253	NDF	Boreal	2003	213	163	3.0[e]	26.7	42.0[f]	*Hill et al.* [2011]
8	FI-Hyy	61.847	24.295	185	NDF	Boreal	2006	500	153	6.7	35.5	6.6[g]	*Tanja et al.* [2003]
9	JP-Tom	42.737	141.521	140	NDF	Boreal[c]	2002	977	—	9.2	13.0	65.0	*Hirata et al.* [2007]
10	ID-Pag	−2.345	114.036	30	BEF	Tropical	2002	1852	—	5.0	26.4	2.8	*Hirano et al.* [2007]
11	TH-Sak	14.492	101.916	543	BEF	Tropical	2002	1813	—	3.7	62.1	24.3	*Kamo et al.* [2002]; *Hirata et al.* [2008]
12	FR-Pue	43.741	3.596	270	BEF	Mediterranean	2008	1116	243	2.9	14.1	39.7	*Rambal et al.* [2003]
13	IT-Cpz	41.705	12.376	9	BEF	Mediterranean	2007	593	294	3.5	89.6	5.4	*Garbulksy et al.* [2008]; *Reichstein et al.* [2007]
14	IT-Col	41.849	13.588	1645	BDF	Mediterranean	2005	954	156	6.4	65.0	10.0[g]	*Valentini et al.* [1996]
15	US-MOz	38.744	−92.200	212	BDF	Mediterranean	2005	1023	256	4.0	7.0	15.0[g]	*Gu et al.* [2006]
16	CA-Oas	53.629	−106.198	580	BDF	Boreal	2003	261	109	2.6	46.0	20.8[f]	*Barr et al.* [2006]; *Krishnan et al.* [2006]
17	DK-Sor	55.487	11.646	40	BDF	Boreal	2004	631	152	5.0	67.5	10.0[g]	*Pilegaard et al.* [2003]
18	CA-Mer	45.409	−75.519	65	BDS	Temperate	2006	1203	174	1.2	63.1	15.9[f]	*Lafleur et al.* [2003]; *Roulet et al.* [2007]
19	US-Ivo	68.487	−155.748	557	BDS	Boreal	2005	202	170	2.5[e]	45.5	18.6	*Oechel et al.* [2000]
20	CA-NS6	55.917	−98.964	271	BDS	Boreal	2002	267	47	3.0[e]	3.4	81.1[g]	*Goulden et al.* [2006]; *McMillan et al.* [2008]
21	AT-Neu	47.116	11.320	970	GRA	Temperate	2003	764	146	6.5	52.5	6.2	*Wohlfahrt et al.* [2008]
22	IE-Dri	51.987	−8.752	187	GRA	Temperate	2004	1341	216	5.2[e]	15.0	50.0	*Montaldo et al.* [2007]; *Peichl et al.* [2011]

[a]The site ID was taken from FLUXNET.
[b]Biome types: needleleaf evergreen forest (NEF), needleleaf deciduous forest (NDF), broadleaf evergreen forest (BEF), broadleaf deciduous forest (BDF), broadleaf deciduous shrub (BDS), grassland (GRA).
[c]The JP-Tom site was categorized as a boreal forest ecosystem for the absence of the temperate needleleaf deciduous forest in the PFTs [*Oleson et al.*, 2010].
[d]Data for growing season calculation are not available.
[e]Data were extracted from a global LAI map based on 10 day synthesis VEGETATION images at 1 km spatial resolution [*Chen et al.*, 2005b, 2012; *Deng et al.*, 2006].
[f]Data acquired from North American Carbon Program.
[g]Data obtained from http://www.fluxdata.org/.

Table 2. Plant Functional Types-Dependent Parameters Used in CLM and DLM for ET Estimation[a]

Biome Type	Climate Zone	CLM		DLM		
		Vc_{max25}:$f(N)$	m	Vc_{max25}:$f(N)$	m	Ω[b]
		(μmol m^{-2} s^{-1})	—	(μmol m^{-2} s^{-1})	—	—
NEF	Temperate	55	6	46.3	5.5	0.55
NEF	Boreal	42	6	41.1	7.3	0.55
NDF	Boreal	29	6	25.5	7.6	0.68
BEF	Tropical	66	9	48.6	9.2	0.63
BEF	Temperate	51	9	39.4	6.0	0.63
BDF	Temperate	30	9	31.0	5.7	0.70
BDF	Boreal	40	9	35.3	8.4	0.70
BDS	Temperate	30	9	23.6	5.3	0.70
BDS	Boreal	19	9	21.3	8.5	0.70
GRA(C3)	Temperate	26	9	25.4	8.3	0.80

[a]The terms Vc_{max25}:$f(N)$, m, and Ω are the leaf maximum carboxylation rate at 25°C constrained by leaf nitrogen, the slope of conductance-to-photosynthesis relationship, and the foliage clumping index, respectively.
[b]Parameters obtained from *Tang et al.* [2007].

energy flux into *LE* and *H* according to the measured Bowen ratio [*Twine et al.*, 2000; *Ingwersen et al.*, 2011].

[8] In this study, the representative simulations of 22 EC towers (Table 1) were selected covering major six biomes across three climate zones: 8 sites in boreal regions, 12 sites in temperate regions, and 2 sites in tropical regions. The JP-Tom site in the temperate zone was categorized as a boreal forest ecosystem because of the absence of the temperate needleleaf deciduous forest in the PFTs we used [*Oleson et al.*, 2010]. For the same reason, five sites that have mediterranean style climates were characterized as in temperate zones.

2.2. Model Description

[9] We estimated water vapor flux using the MT equation and the PM equation in two land surface models, respectively. One is CLM4 [*Bonan et al.*, 2011; *Lawrence et al.*, 2011; *Oleson et al.*, 2010] in CESM version 1.0.3. We revised the modules on two-stream radiative transfer, leaf photosynthesis, and canopy scaling according to *Bonan et al.* [2011]. The other model is DLM, which is an updated version of EASS by *Chen et al.* [2007a] including an improved coupled nitrogen-carbon dynamics module and a vegetation dynamic model with a state-of-art phenology module. DLM has been coupled to CESM 1.0.3 by replacing the original photosynthesis and energy flux modules with EASS-based formulations and optimizing the parameters. These two LSMs adopt identical calculation approaches in their biogeophysical modules except for ET estimation, including the flux-gradient approach in modeling sensible heat flux, the stomatal resistance model by *Ball et al.* [1987], and the photosynthesis model by *Farquhar et al.* [1980] and *Collatz et al.* [1991]. In both of LSMs, leaf photosynthesis is linked to transpiration through the Ball-Woodrow-Berry stomatal model. In addition, both models use the two-leaf upscaling strategy in simulating canopy photosynthesis, but this strategy is only adapted by DLM to model energy flux.

[10] We employed the published parameters for CLM, e.g., the leaf maximum carboxylation rate at 25°C constrained by leaf nitrogen [*Bonan et al.*, 2011] and the slope of conductance-to-photosynthesis relationship [*Oleson et al.*, 2010] in Table 2, and optimized some PFTs-dependent parameters about biochemistry and biophysics for DLM (Table 2) because of its updating. Adopting the parameter optimization algorithm by *Chen et al.* [2011a], we first identified the sensitive parameters to photosynthesis and energy fluxes by analyzing the response of parameters by random sampling of parameters within their possible ranges. Then we applied the ensemble Kalman filter data model synthesis approach, which encompasses both model parameter optimization and data assimilation, to optimize these parameters by minimizing the difference between observations and predications [*Mo et al.*, 2008]. Based on a 102 site-years analysis, we combined the parameters for each PFT to perform a process-based analysis at the global scale. The key PFTs-dependent parameters in ET estimates are shown in Table 2 for both LSMs.

[11] We considered that the effects of using the MT and PM equations in land surface modeling systems could be assessed by comparing the estimates using CLM and DLM, respectively. Three simulations were performed to determine the biases arising for the ET estimation: MT, a control simulation with the MT equation and the one-leaf strategy in water vapor flux estimation by CLM4, which is revised according to *Bonan et al.* [2011] based on the public release code in CESM1.0.3; PM2L, a simulation with the PM equation and a two-leaf strategy in carbon and energy fluxes simulation (default DLM); and PM1L, a simulation in which the two-leaf strategy has been replaced by a one-leaf strategy in ET estimation and kept the other module unanimous with the default DLM. The design of PM1L is aimed at distinguishing the effects of the two canopy upscaling strategies on ET estimation. We only utilized the biogeophysical module for each of the simulation so that the estimates were unaffected by biases in biogeochemistry (e.g., carbon-nitrogen coupling) [*Bonan et al.*, 2011; *Lawrence et al.*, 2011].

2.2.1. Evapotranspiration

[12] 1. Mass transfer equation

In CLM, the water vapor flux is determined by vegetation and ground specific humidity differences simultaneously in the case of a vegetated surface and is the sum of the water vapor transfer from the canopy to the canopy air for the vegetation (E_{veg}^{evap}) and from the ground to the canopy air for the ground (E_{grnd}^{evap}) [*Oleson et al.*, 2010]:

$$ET = E_{veg}^{evap} + E_{grnd}^{evap} \tag{1}$$

[13] The water vapor flux from vegetation is determined by water vapor flux from wetted leaf and stem area ($f'' E_{\mathrm{veg}}^{\mathrm{pot}}$) and transpiration from the dry leaf surface ($f''_{dry} E_{\mathrm{veg}}^{\mathrm{pot}} + W_{can}/\Delta t$) [*Oleson et al.*, 2010]

$$E_{veg}^{evap} = \min\left(f'' E_{\mathrm{veg}}^{\mathrm{pot}}, f''_{dry} E_{\mathrm{veg}}^{\mathrm{pot}} + W_{can}/\Delta t\right) \tag{2}$$

$$E_{veg}^{\mathrm{pot}} = \frac{\rho_{atm}\left(q_{T_{veg}}^{sat} - q_s\right)}{r_b} \tag{3}$$

where $E_{\mathrm{veg}}^{\mathrm{pot}}$ is the potential evaporation from wet foliage per unit wetted area, f'' and f''_{dry} are fractions of potential

evaporation from leaf and through transpiration (see below), respectively, $W_{can}/\Delta t$ is the water stored on the canopy at each time step, r_b is the leaf boundary layer resistance, q_s is the canopy specific humidity (in kg kg^{-1}) affected by a combination of heat conductance and specific humidity of air, leaf, and ground, and $q^{sat}_{T_{veg}}$ is the saturation specific humidity at the vegetation temperature (T_{veg}) [*Flatau et al*., 1992; *Oleson et al*., 2010]. Similarly, the expression for the actual specific humidity at the ground surface (q_{grnd}) can be substituted to obtain the water vapor flux from the ground beneath the canopy (E^{evap}_{grnd}) [*Lawrence et al*., 2011; *Oleson et al*., 2010]:

$$E^{evap}_{grnd} = \frac{\rho_{atm}\beta_{soi}\left(q_{grnd} - q_s\right)}{r'_{aw} + r_{litter}} \tag{4}$$

where β_{soi} is an empirical function of soil water, r'_{aw} is the aerodynamic resistance to water vapor transfer between the ground and the canopy air, and r_{litter} is a resistance of the plant litter layer. The value of q_{grnd} is assumed to be proportional to the saturation specific humidity at the ground surface temperature, and the proportion is a weighted combination of the soil water matric potential of the top soil layer and the fraction of ground covered by snow. See *Oleson et al*. [2010] for more details.

[14] 2. Penman-Monteith equation

In DLM, canopy-scale ET can be expressed as [*Chen et al*., 2007a] follows:

$$\mathrm{ET} = T_C + E_C + E_S \tag{5}$$

where T_C is the transpiration from the canopy, E_C is the water vapor from the canopy including evaporation of rain and sublimation of snow, and E_S is the combination of evaporation and sublimation from the soil surface.

[15] Each ET component was calculated using the PM equation expressed in a general form as given below [*Chen et al*., 2005a; *Chen et al*., 2007a; *Govind et al*., 2009]:

$$ET_i = \frac{\Delta \cdot R_{n_{\hat{i}}} + \rho_{atm} c_p \left(e^{sat}_{\hat{i}} - e_{\hat{i}}\right)/r_{a\hat{i}}}{\lambda_v[\Delta + \gamma(1 + r_{c\hat{i}}/r_{a\hat{i}})]}\delta t \tag{6}$$

where ET_i is the amount of water evaporated from the surface of the leaf or soil (layer $i = 1$ or 2) or transported from the leaf over the period δt, $R_{n_{\hat{i}}}$ is the net radiation available on the surface of layer i, which is calculated from the shortwave and longwave radiation absorbed by the surface, ρ_{atm} is the density of moist air, c_p is the specific heat of air at a constant pressure, $e^{sat}_{\hat{i}}$ is the saturated water vapor pressure in Pa, which is calculated from an eighth-order polynomial function of the temperature of each layer [*Flatau et al*., 1992], $e_{\hat{i}}$ is the actual water vapor pressure, λ_v is the latent heat of vaporization of water, Δ is the slope of the saturated vapor pressure-temperature curve, γ is the psychrometric constant, $r_{c\hat{i}}$ is the sunlit/shaded stomatal or soil resistance to vapor transport, and $r_{a\hat{i}}$ is the aerodynamic resistance to vapor transport for layer i. Details can be found in the supplemental material and *Chen et al*. [2007a].

2.2.2. Canopy Upscaling

[16] 1. Two-leaf strategy

The DLM calculates canopy evaporation (E_C) for sunlit and shaded parts separately by adopting the sunlit and shaded leaf area indices ($\mathrm{LAI_{sun}}$ and $\mathrm{LAI_{sha}}$). The leaf stratification strategy for E_C is [*Chen et al*., 2007a]

$$E_C = E_{C\,sun}LAI_{sun} + E_{C\,sha}LAI_{sha} \tag{7}$$

$$LAI_{sun} = \frac{1 - \exp[-G(\theta)\cdot\Omega\cdot LAI/\mu]}{G(\theta)/\mu} \tag{8}$$

$$LAI_{sha} = LAI - LAI_{sun} \tag{9}$$

where $G(\theta)$ is the foliage projection coefficient taken as 0.5 assuming a spherical leaf angle distribution and μ is the cosine of the solar zenith angle. The clumping index (Ω) characterizes the leaf spatial distribution pattern in terms of the degree of its deviation from the random case. This approach is also applied to modeling transpiration (T_C).

[17] 2. One-leaf strategy

Analogous to equations 8 and 9, CLM separates the canopy into two parts ($\mathrm{LAI_{sun}}$ and $\mathrm{LAI_{sha}}$) in photosynthesis and further in stomatal resistance estimations[*Oleson et al*., 2010] but adopts the foliage projection area as a function of the departure of leaf angles from a random distribution and ignores the impact of the clumping index. To combine the effects from both sunlit and shaded leaves in the ET estimation, CLM uses a fraction of potential evaporation through transpiration (f''_{dry})[*Oleson et al*., 2010]in the following:

$$f''_{dry} = \frac{f_{dry}r_b}{LAI}\left(\frac{LAI_{sun}}{r_b + r^{sun}_s} + \frac{LAI_{sha}}{r_b + r^{sha}_s}\right) \tag{10}$$

where f_{dry} is the fraction of leaves that are dry and depends on canopy water storage, LAI, and stem area index. r^{sun}_s and r^{sha}_s are the sunlit and shaded stomatal resistances, respectively, both obtained using the Ball-Woodrow-Berry conductance model [*Oleson et al*., 2010].

[18] In the one-leaf strategy of the PM equation (PM1L), we replaced the value of f_{dry} with 1.0 and removed r_b in equation 10 to gain the one-leaf stomatal resistance from r^{sun}_s and r^{sha}_s. The water vapor flux was scaled up to the canopy level with an exponential equation from that of an unshaded leaf [*Alton et al*., 2007; *Mercado et al*., 2007; *Sprintsin* et al., 2012], which is analogous to the calculation of half-hourly canopy evaporation and transpiration in the two-leaf strategy (equations 7 and 8). The one-leaf strategy in the E_C estimation follows

$$E_C = f_{scale}E_{C0} \tag{11}$$

$$f_{scale} = \frac{1 - \exp(-k\cdot LAI)}{k} \tag{12}$$

where Ec_0 is the evaporation from an unshaded leaf and f_{scale} is a multiplicative factor, in which the canopy photosynthetically active radiation (PAR) extinction coefficient k is taken to be 0.5. The same approach is also used for T_C estimate.

2.3. Model Simulations

[19] Off-line single point simulations with a 30 min time step were performed using observed meteorological data and land surface data. The half-hourly meteorological data were measured at the EC towers, including downwelling solar radiation (in W m^{-2}), precipitation (in mm), wind speed (in m s^{-1}), air temperature (in K), and relative humidity (in %). Missing half-hourly values of these key model inputs due to periods of instrument failure were gap filled by linear interpolation of gaps less than 2 h. Larger gaps were filled by applying a

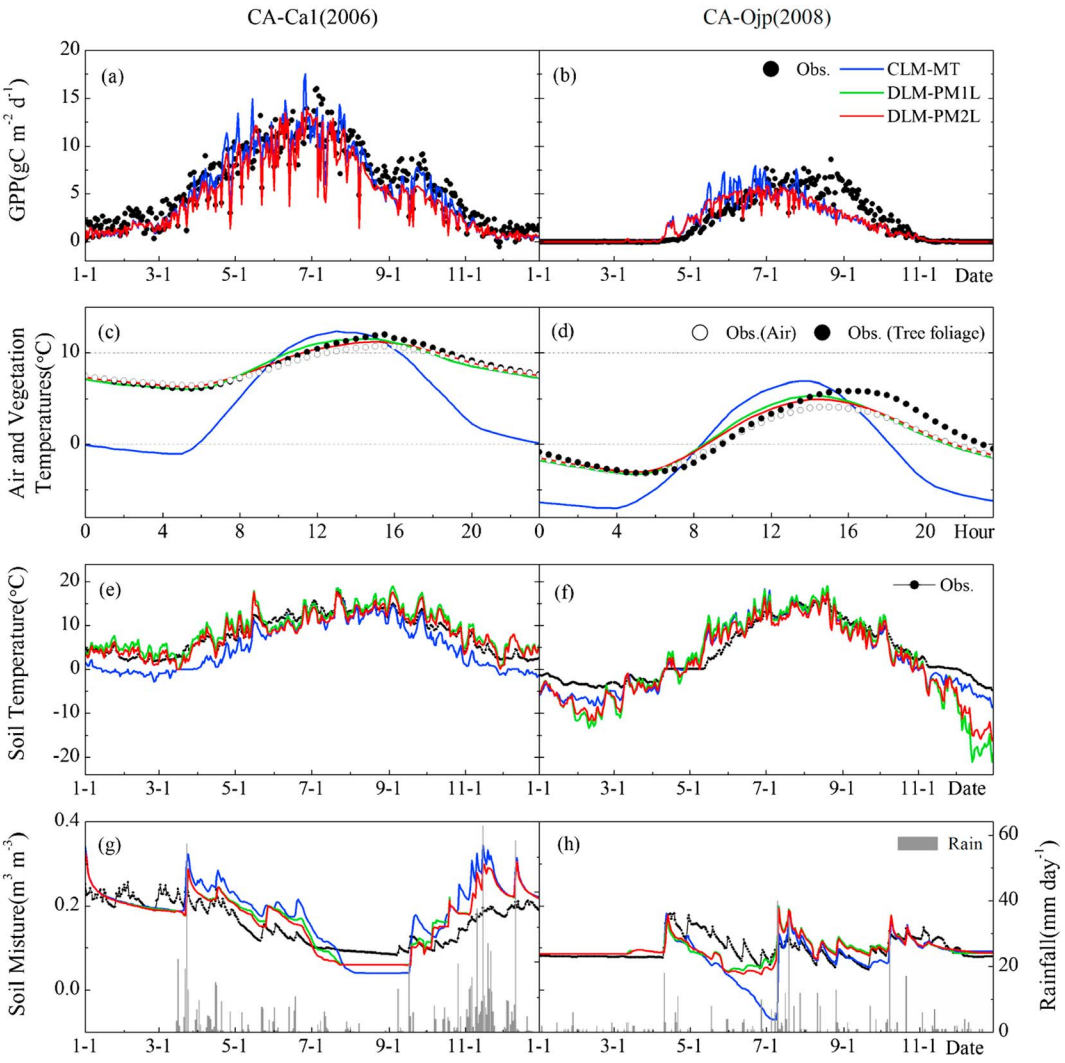

Figure 1. Simulated (color lines) and observed (dark lines and symbols) vegetation and soil temperatures and soil moistures for two site-years (CA-Ca1 (2006) in the left-hand side and CA-Ojp (2008) in the right-hand side). (a,b) Daily gross primary production (GPP); (c,d) annually averaged diurnal composites of simulated vegetation temperature (lines), observed tree foliage temperature (filled circles), and observed air temperature above the canopy (open circles); (e,f) daily averaged soil temperature in the surface layer (10 cm depth); and (g,h) daily averaged soil moisture in surface layer (10 cm depth, lines) and daily cumulative precipitation (bars).

simple interpolation technique of mean diurnal variation [*Falge et al*., 2001; *Moffat et al*., 2007].

[20] For each site, the soil texture (i.e., percentages of sand and clay) were obtained from the site's information or published articles (Table 1). We adopted soil property data sets (i.e., soil color and organic matter content at each soil depth) provided by CESM1.0.3 as a source of land surface data for the year 2000 [*Lawrence et al*., 2011; *Stöckli et al*., 2008]. Soil state variables (e.g., soil temperature and moisture) of each site for the off-line simulations were initialized by spinning up for 200 years with repeat years 1982–2001 atmospheric forcing data set from the National Centers for Environmental Prediction reanalysis data set [*Qian et al*., 2006] provided by NCAR.

[21] Monthly LAI values for each site were extracted from a global LAI map based on 10 day synthesis VEGETATION images at 1 km spatial resolution in 2003, which has been corrected based on a global clumping index map produced from the multiangle observation of POLDER 1, 2, and 3 sensors [*Chen et al*., 2005b, 2012; *Deng et al*., 2006]. We corrected the monthly LAI for each site according to the LAI_{max} value (Table 1) supplied by the biological information for each site. Although the years for which available supplementary land surface data are available do not always correspond to the years being modeled, we assumed that the data are adequate for our water vapor flux modeling.

2.4. Model Performance

[22] We quantified model performance using statistical analysis based on half-hourly *LE* for each model-data pair. Model-data mismatch was evaluated using bias, root-mean-square error (RMSE) [*Willmott*, 1982; *Willmott and Matsuura*, 2005; *Willmott et al*., 1985], normalized mean absolute error (NMAE) [*Marlin*, 2004], as well as index of agreement

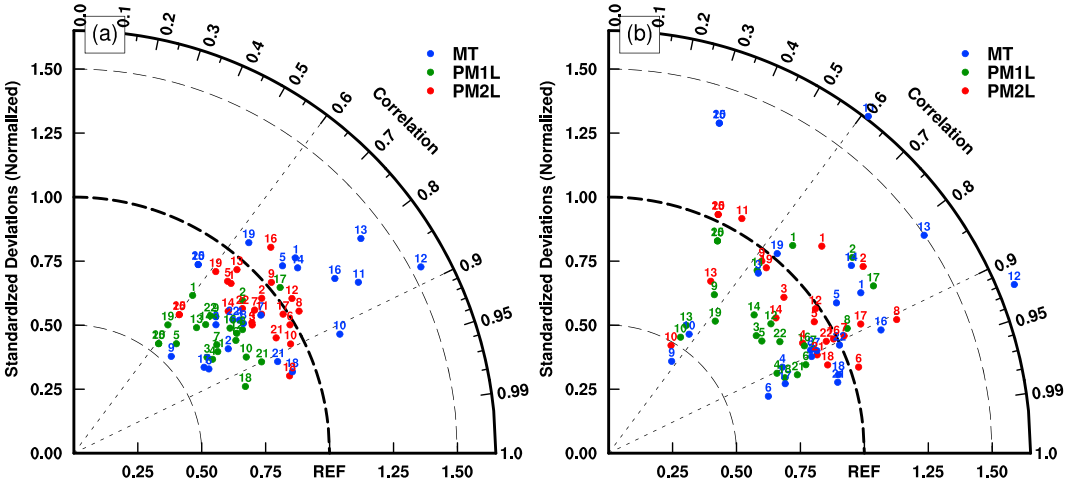

Figure 2. Performance of the three models for the 22 selected tower sites (number 1–22). Statistics in the Taylor diagram are derived from simulated and observed *LE* fluxes of site-year: (a) half-hourly and (b) daily averaged. Color regimes: blue for MT, green for PM1L, and red for PM2L. An ideal model would have a standard deviation ratio (σ_{norm}) of 1.0 and a correlation coefficient of 1.0 (REF, the reference point).

(IA) [*Vörösmarty et al.*, 1996; *Willmott*, 1982]. The skills were calculated by the following:

$$\text{Bias} = \sum_{i=1}^{n}(P_i - O_i)/n \tag{13}$$

$$\text{RMSE} = \sqrt{\sum_{i=1}^{n}(P_i - O_i)^2/n} \tag{14}$$

$$\text{NMAE} = \sum_{i=1}^{n}|O_i - P_i|/\left(n\overline{O}\right) \tag{15}$$

and

$$\text{IA} = 1 - \sum_{i=1}^{n}(P_i - O_i)^2 / \sum_{i=1}^{n}\left(|P_i - \overline{O}| + |O_i - \overline{O}|\right)^2 \tag{16}$$

where P_i and O_i denote predicated and observed values, respectively; $\bar{O}$ is the mean of the observed data.

[23] A final characterization of model performance uses the Taylor diagram [*Taylor*, 2001], in which a single point indicate the linear correlation coefficient (R) and the ratio of the standard deviations between the prognosis and the observation ($\sigma_{\text{norm}} = \sigma_p/\sigma_o$), along with the root-mean-square difference of the two patterns on a two-dimensional plot. An ideal model would have a standard deviation ratio of 1.0 and a correlation coefficient of 1.0, i.e., the reference point on the x axis. Taylor skill (S) is a single value summary of a Taylor diagram where unity indicates perfect agreement with observations. More generally, each point for any arbitrary data group [*Schwalm et al.*, 2010; *Taylor*, 2001] can be scored as follows:

$$S = 2(1 + R)/(\sigma_{norm} + 1/\sigma_{norm})^2 \tag{17}$$

3. Results

3.1. Estimates of Important Variables

[24] Key variables used to simulate water vapor flux are derived from the outputs of other modules in both LSMs, as the stomatal resistance is based on the Ball-Woodrow-Berry stomatal model (equation S25 in the supporting information) in equations 6 and 10, the leaf and soil temperatures (equations S26–S29) used to calculating saturation specific humidity in the equations 3 and 4 and saturation vapor pressure in the equation 6, and the soil moisture distribution (equation S30) in simulating soil moisture dynamics to limit soil evaporation (β_{soi} in equation 4 and $r_{c\hat{i}}$ in equation 6). We drew a comparison between these modeled and measured variables to clarify a potential module structure effect on the accuracy of ET estimation. Examples were presented for CA-Ca1 and CA-Ojp (Figure 1). These two needleleaf evergreen forests in temperate and boreal regions, respectively, provided complete observations, including the tree foliage temperature, in all sites we selected. We only show one preventative year at each site since the behavior is comparable from year to year in simulation.

[25] In the Ball-Woodrow-Berry stomatal model (equation S25), the stomatal resistance is calculated based on the photosynthetic rate, which derived from *Farquhar* photosynthesis mode in both LSMs. As shown in Figures 1a and 1b, the daily gross primary productions (GPP) simulated by CLM and DLM were comparable to the observations in both sites, excepting that both LSMs underestimated the values at CA-Ojp from August to October in 2008. Annual averaged diurnal variations of modeled vegetation temperatures of these two sites were higher than air temperature at midday (Figures 1c and 1d). The errors of DLM-PM1L and DLM-PM2L estimations were usually less than 1°C, but CLM errors far exceeded 2°C. Moreover, all models did not capture the elevated temperature of tree foliage in the afternoon. DLM-PM1L and DLM-PM2L adopted the same approach as that used in CLM to estimate soil temperature (equation S29). As shown in Figures 1e and 1f, modeled daily averaged soil temperatures (10 cm depth) agreed well with observations during the warm days for both sites. The models explained 70–96% and 80–83% of the variance at CA-Cal and CA-Ojp, respectively, from April to October (n = 214 for each site in each model). However, the soil temperatures were underestimated during the cold months especially in CA-Ojp. The average biases of this site were −2.7°C, −5.9°C, and −5.0°C for MT, PM1L, and PM2L (n = 151 for each model), respectively.

Table 3. Comparison of Model Performance in Estimating Latent Heat Flux (*LE*) at Half-Hourly and Daily Time Scales[a]

		MT				PM1L				PM2L			
		Slope	RMSE	NMAE	IA	Slope	RMSE	NMAE	IA	Slope	RMSE	NMAE	IA
Number	Site ID		($W\ m^{-2}$)				($W\ m^{-2}$)				($W\ m^{-2}$)		
						Half-Hourly							
1	CA-Ca1	**0.87**	34.7	0.69	**0.85**	0.46	37.4	0.73	0.74	0.61	**34.0**	**0.66**	0.81
2	DE-Tha	0.60	**38.8**	**0.59**	0.87	0.66	43.8	0.67	0.85	**0.73**	42.0	0.64	**0.87**
3	ES-ES1	0.56	42.5	0.60	0.81	0.52	39.2	0.53	0.83	**0.70**	**35.4**	**0.47**	**0.88**
4	US-Ho1	0.65	38.6	0.79	0.87	0.54	**36.3**	0.69	0.86	**0.70**	36.4	**0.65**	**0.89**
5	CN-Qia	0.53	65.7	0.54	0.84	0.63	62.5	0.53	0.88	**0.85**	**55.1**	**0.47**	**0.93**
6	CA-Ojp	**0.82**	31.1	0.78	**0.85**	0.40	**30.3**	0.78	0.75	0.60	31.7	**0.71**	0.80
7	CA-NS1	**0.73**	**26.2**	0.68	**0.89**	0.56	26.7	0.66	0.86	0.71	27.3	**0.61**	0.88
8	FI-Hyy	0.66	27.8	0.76	0.86	0.66	25.5	0.62	0.88	**0.88**	**24.2**	**0.56**	**0.92**
9	JP-Tom	0.38	61.3	0.68	0.73	0.56	57.7	0.64	0.81	**0.77**	**56.2**	**0.60**	**0.86**
10	ID-Pag	**1.04**	73.4	0.37	**0.95**	0.67	81.2	0.39	0.91	0.85	**68.7**	**0.32**	0.94
11	TH-Sak	**1.11**	73.0	0.78	0.89	0.56	**57.3**	0.58	0.86	0.73	58.4	**0.56**	**0.89**
12	FR-Pue	1.36	48.3	0.82	0.88	0.64	**33.3**	0.62	0.88	**0.85**	35.8	**0.59**	**0.89**
13	IT-Cpz	**1.12**	40.1	0.90	**0.85**	0.48	**31.6**	**0.71**	0.80	0.64	35.7	0.75	0.81
14	IT-Col	**0.88**	35.6	0.83	**0.87**	0.52	33.9	0.74	0.81	0.60	**32.8**	**0.71**	0.84
15	US-MOz	**0.49**	90.8	1.41	0.72	0.33	**79.5**	1.26	0.70	0.41	80.1	**1.25**	**0.74**
16	CA-Oas	**1.02**	32.0	0.79	**0.89**	0.61	**28.3**	0.66	0.86	0.77	37.8	**0.63**	0.82
17	DK-Sor	0.51	48.2	0.75	0.84	0.81	52.5	0.75	0.88	**0.82**	**44.6**	**0.64**	**0.91**
18	CA-Mer	**0.85**	26.5	0.36	0.96	0.67	33.5	0.44	0.93	0.84	**26.0**	**0.35**	**0.97**
19	US-Ivo	**0.68**	21.1	1.18	**0.79**	0.37	**19.8**	1.02	0.70	0.55	20.2	**1.01**	0.77
20	CA-NS6	**0.49**	90.8	1.41	0.72	0.33	**79.5**	1.26	0.70	0.41	80.1	**1.25**	**0.74**
21	AT-Neu	**0.80**	**30.9**	**0.41**	**0.95**	0.73	34.5	0.46	0.93	0.79	37.4	0.46	0.93
22	IE-Dri	0.62	42.3	0.63	0.85	0.53	45.9	0.66	0.80	**0.66**	**41.6**	**0.57**	**0.86**
						Daily							
1	CA-Ca1	**0.99**	**16.4**	**0.42**	**0.87**	0.72	22.1	0.52	0.76	0.83	19.2	0.46	0.82
2	DE-Tha	0.79	**20.2**	**0.43**	**0.88**	0.95	24.9	0.48	0.86	**1.00**	23.4	0.44	0.88
3	ES-ES1	0.59	24.3	0.43	0.69	0.58	21.6	0.39	0.73	**0.69**	**17.5**	**0.29**	**0.82**
4	US-Ho1	0.68	**15.3**	0.42	0.92	0.66	15.9	0.41	0.92	**0.76**	16.1	**0.39**	**0.93**
5	CN-Qia	0.62	32.9	0.40	0.83	0.77	25.6	0.30	0.91	**0.98**	**15.7**	**0.18**	**0.97**
6	CA-Ojp	**0.89**	13.4	0.50	0.90	0.60	13.3	0.45	0.86	0.80	**11.5**	**0.38**	**0.91**
7	CA-NS1	0.81	**10.7**	0.40	0.94	0.80	11.3	0.35	0.93	**0.92**	11.0	**0.34**	**0.94**
8	FI-Hyy	0.79	14.9	0.56	0.90	**0.93**	**12.7**	0.41	0.93	1.13	13.0	**0.38**	**0.94**
9	JP-Tom	0.25	43.3	0.60	0.60	0.41	42.6	0.58	0.69	**0.60**	**38.2**	**0.51**	**0.77**
10	ID-Pag	**0.31**	**46.1**	**0.24**	**0.68**	0.28	68.5	0.43	0.57	0.24	53.0	0.30	0.60
11	TH-Sak	**1.02**	44.4	0.63	0.59	0.58	**21.6**	**0.30**	**0.76**	0.52	25.3	0.32	0.70
12	FR-Pue	1.59	29.7	0.66	0.85	0.63	**17.8**	0.40	0.87	**0.81**	18.6	**0.40**	**0.88**
13	IT-Cpz	**1.23**	21.3	0.65	**0.78**	0.30	**15.3**	**0.50**	0.66	0.40	16.4	0.51	0.71
14	IT-Col	**0.95**	17.7	0.53	0.87	0.57	16.8	0.52	0.82	0.65	**14.8**	**0.46**	**0.87**
15	US-MOz	**0.43**	48.0	0.94	0.57	0.43	**33.2**	**0.66**	**0.69**	0.43	36.3	0.73	0.67
16	CA-Oas	**1.06**	15.0	0.52	0.93	0.77	12.8	0.38	0.93	0.88	**12.0**	**0.36**	**0.94**
17	DK-Sor	0.69	20.8	0.44	0.90	1.04	24.8	0.41	0.91	**0.99**	**19.2**	**0.33**	**0.94**
18	CA-Mer	**0.90**	**14.1**	**0.25**	**0.97**	0.69	21.0	0.39	0.91	0.86	16.3	0.28	0.95
19	US-Ivo	**0.66**	13.1	0.91	**0.80**	0.42	**12.8**	0.83	0.74	0.62	12.8	**0.83**	0.80
20	CA-NS6	**0.43**	48.0	0.94	0.57	0.43	**33.2**	**0.66**	**0.69**	0.43	36.3	0.73	0.67
21	AT-Neu	**0.90**	**12.1**	**0.24**	**0.97**	0.74	18.1	0.38	0.92	0.82	17.2	0.34	0.94
22	IE-Dri	**0.90**	18.7	0.41	0.88	0.67	20.1	0.42	0.83	0.85	**15.3**	**0.31**	**0.91**

[a]Bold numbers show the best of the three models for each diagnostic and site.

We compared daily averaged soil moisture contents at a soil depth of 10 cm and precipitation at CA-Cal and CA-Ojp (Figures 1g and 1h). The simulated soil moisture contents in the surface layer agreed well with the measurements, excepting that CLM underestimated soil moisture content in the middle of the year 2008 at CA-Ojp. Peak values of simulated and observed soil moisture values were associated with high daily accumulated precipitation, which indicate that changes in soil water content in response to rainfall events and drying were reasonably captured by the three models. Similar results were also observed in other sites. These comparisons suggest that with the same methods in modeling GPP, soil temperature, and soil moistures, there are no obvious discrepancy in these key variables used to simulate water vapor flux in all three models. The differences existed in leaf temperature estimates, which are calculated during the iterated process in modeling canopy energy fluxes in three simulation scenarios.

3.2. Model-Data Agreement on Half-Hourly and Daily Time Scales

[26] Comparisons between modeled and observed *LE* in Figure 2 and Table 3 provided an overview of performances among models on half-hourly and daily time scales. Overall, the three models had a similar *R* range within the same time scale, but PM2L performed better than MT and PM1L with σ_{norm} closer to 1, smaller RMSE and NMAE, and greater IA.

[27] Half-hourly *LE* was well quantified by the three models for the 22 tower sites. As shown in Figure 2a, model fittings to the observed data ranged in *R* values of 0.55–0.93, 0.59–0.93 and 0.61–0.94 for MT, PM1L and PM2L, and in σ_{norm} of

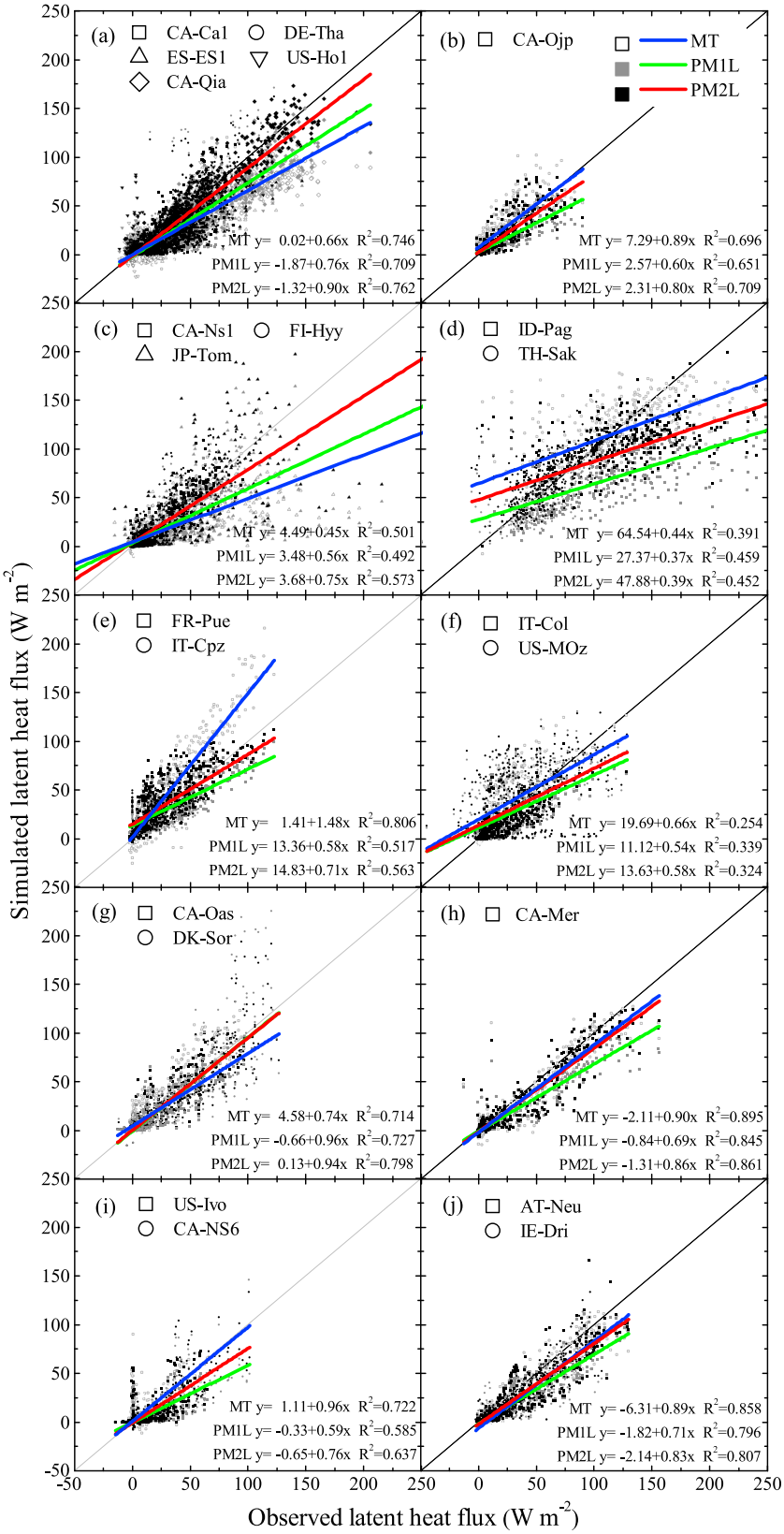
(a) CA-Ca1 DE-Tha ES-ES1 US-Ho1 CA-Qia
MT y= 0.02+0.66x R²=0.746
PM1L y= -1.87+0.76x R²=0.709
PM2L y= -1.32+0.90x R²=0.762
(b) CA-Ojp
MT
PM1L
PM2L
MT y= 7.29+0.89x R²=0.696
PM1L y= 2.57+0.60x R²=0.651
PM2L y= 2.31+0.80x R²=0.709
(c) CA-Ns1 FI-Hyy JP-Tom
MT y= 4.49+0.45x R²=0.501
PM1L y= 3.48+0.56x R²=0.492
PM2L y= 3.68+0.75x R²=0.573
(d) ID-Pag TH-Sak
MT y= 64.54+0.44x R²=0.391
PM1L y= 27.37+0.37x R²=0.459
PM2L y= 47.88+0.39x R²=0.452
(e) FR-Pue IT-Cpz
MT y= 1.41+1.48x R²=0.806
PM1L y= 13.36+0.58x R²=0.517
PM2L y= 14.83+0.71x R²=0.563
(f) IT-Col US-MOz
MT y= 19.69+0.66x R²=0.254
PM1L y= 11.12+0.54x R²=0.339
PM2L y= 13.63+0.58x R²=0.324
(g) CA-Oas DK-Sor
MT y= 4.58+0.74x R²=0.714
PM1L y= -0.66+0.96x R²=0.727
PM2L y= 0.13+0.94x R²=0.798
(h) CA-Mer
MT y= -2.11+0.90x R²=0.895
PM1L y= -0.84+0.69x R²=0.845
PM2L y= -1.31+0.86x R²=0.861
(i) US-Ivo CA-NS6
MT y= 1.11+0.96x R²=0.722
PM1L y= -0.33+0.59x R²=0.585
PM2L y= -0.65+0.76x R²=0.637
(j) AT-Neu IE-Dri
MT y= -6.31+0.89x R²=0.858
PM1L y= -1.82+0.71x R²=0.796
PM2L y= -2.14+0.83x R²=0.807
Simulated latent heat flux (W m-2)
Observed latent heat flux (W m-2)
-50 0 50 100 150 200 250

Figure 3

Table 4. Bias, Correlation Coefficient (R), and Root-Mean-Square Error (RMSE) of Half-hourly Latent Heat Flux (LE) With Respect to Individual Months and Seasons in Temperate and Boreal Sites

	MT			PM1L			PM2L		
	Bias	R	RMSE	Bias	R	RMSE	Bias	R	RMSE
Months/Seasons	(W m^{-2})		(W m^{-2})	(W m^{-2})		(W m^{-2})	(W m^{-2})		(W m^{-2})
Jan.	−6.3(±27.6)[a]	**0.38**(±0.27)	23.18(±16.61)	−4.1(±28.1)	0.32(±0.23)	20.98(±19.56)	−3.9(±27.9)	0.33(±0.24)	**20.78**(±19.38)
Feb.	−7.1(±32.9)	**0.55**(±0.23)	26.70(±20.38)	−7.3(±35.1)	0.46(±0.26)	25.68(±25.02)	−7.0(±34.5)	0.47(±0.26)	**25.08**(±24.72)
Mar.	−5.4(±44.3)	**0.57**(±0.25)	35.64(±27.02)	−6.8(±45.1)	0.53(±0.26)	**34.81**(±29.78)	−5.3(±44.7)	0.53(±0.26)	34.88(±28.73)
Apr.	−2.5(±49.0)	**0.70**(±0.17)	44.14(±22.53)	−9.8(±45.8)	0.65(±0.24)	40.22(±25.22)	−6.4(±43.9)	0.66(±0.25)	**38.88**(±22.82)
May	−1.2(±52.3)	**0.76**(±0.20)	48.72(±19.30)	−12.2(±50.5)	0.71(±0.19)	48.81(±18.69)	−5.4(±49.8)	0.75(±0.19)	**46.98**(±18.67)
Mar.	−5.4(±44.3)	**0.57**(±0.25)	35.64(±27.02)	−6.8(±45.1)	0.53(±0.26)	**34.81**(±29.78)	−5.3(±44.7)	0.53(±0.26)	34.88(±28.73)
Apr.	−2.5(±49.0)	**0.70**(±0.17)	44.14(±22.53)	−9.8(±45.8)	0.65(±0.24)	40.22(±25.22)	−6.4(±43.9)	0.66(±0.25)	**38.88**(±22.82)
May	−1.2(±52.3)	**0.76**(±0.20)	48.72(±19.30)	−12.2(±50.5)	0.71(±0.19)	48.81(±18.69)	−5.4(±49.8)	0.75(±0.19)	**46.98**(±18.67)
Jun.	−8.2(±67.0)	0.81(±0.07)	60.80(±29.42)	−8.0(±53.5)	0.78(±0.09)	52.41(±15.35)	3.7(±53.8)	**0.81**(±0.09)	**52.14**(±17.61)
Jul.	−0.2(±63.0)	0.81(±0.08)	59.16(±22.75)	−14.0(±59.2)	0.76(±0.14)	58.21(±19.73)	−1.8(±56.5)	**0.83**(±0.15)	**53.65**(±18.33)
Aug.	−3.3(±58.2)	0.78(±0.08)	54.44(±23.61)	−8.6(±56.4)	0.75(±0.10)	54.00(±21.31)	2.2(±56.3)	**0.79**(±0.11)	**53.29**(±19.36)
Sep.	−2.5(±50.5)	0.75(±0.09)	46.16(±21.31)	−2.9(±43.2)	0.74(±0.12)	40.90(±14.15)	2.7(±42.6)	**0.77**(±0.12)	**40.23**(±13.96)
Oct.	−6.2(±39.9)	0.63(±0.16)	36.74(±21.37)	−2.7(±34.6)	0.64(±0.17)	**31.42**(±17.35)	−0.2(±35.1)	**0.68**(±0.17)	31.91(±16.48)
Nov.	−6.4(±34.2)	**0.54**(±0.22)	27.72(±21.07)	−2.4(±32.2)	0.47(±0.23)	**23.70**(±22.24)	−2.1(±31.2)	0.47(±0.25)	23.93(±20.40)
Dec.	−6.7(±27.6)	**0.40**(±0.27)	22.85(±16.65)	−3.2(±27.5)	0.34(±0.25)	**21.48**(±17.33)	−2.7(±30.1)	0.34(±0.26)	23.51(±18.85)
Winter[b]	−6.7(±29.3)	**0.44**(±0.22)	24.67(±17.21)	−4.8(±30.3)	0.35(±0.22)	**23.06**(±20.31)	−4.4(±30.9)	0.35(±0.23)	23.77(±20.24)
Spring	−2.2(±48.7)	**0.72**(±0.17)	43.93(±21.50)	−9.6(±47.3)	0.68(±0.18)	42.87(±22.68)	−5.7(±46.2)	0.69(±0.19)	**41.59**(±21.70)
Summer	−1.5(±63.0)	0.79(±0.08)	58.68(±24.03)	−10.2(±56.5)	0.75(±0.10)	55.24(±17.90)	1.4(±55.6)	**0.81**(±0.11)	**53.34**(±17.55)
Fall	−5.0(±42.1)	0.70(±0.12)	38.19(±19.63)	−2.7(±37.0)	0.71(±0.12)	33.89(±15.63)	0.1(±36.7)	**0.72**(±0.12)	**33.61**(±15.00)
All year	−3.1(±47.6)	0.77(±0.10)	43.66(±19.62)	−6.8(±44.1)	0.75(±0.10)	41.60(±16.80)	−2.2(±43.6)	**0.78**(±0.10)	**40.72**(±16.17)

[a]Values in parentheses are ±1 standard deviation.
[b]Winter is given by December, January, and February with divided 1 year into four seasons.

0.54–1.54, 0.54–1.03, and 0.68–1.11, respectively. Note that although these models had similar R values, values of σ_{norm} in PM2L were close to unity, i.e., the reference point (REF on the x axis). Figure 2 shows a smaller estimation error of PM2L compared with MT and PM1L. Overall agreements across the selected 22 sites were better using the PM equation than using the MT equation, with NMAE and IA values being close to zero and 1.0, respectively, for PM2L on average.

[28] By averaging half-hourly LE into a daily time scale, the performance of the PM equation was more robust than the MT equation (Figure 3). The R^2 of daily LE were larger for the PM equation (PM1L and PM2L) compared to the MT equation at most forest sites (Figures 3a–3g), varying from 0.25–0.74 (MT) to 0.34–0.73 (PM1L) and 0.32–0.80 (PM2L), except for two broadleaf evergreen forests located in the temperate climate zone (FR-Pue and IT-Cpz, Figure 3e). The LE values of this PFT were overestimated by the MT equation as indicated by a slope >1. The simulation biases using the two equations for shrubs (Figures 3h and 3i) and grasslands (Figure 3j) were similar. A further improvement in both correlation and variability was achieved using the two-leaf strategy with the PM equation. The averaged slope of daily LE for various plant functional types increased from 0.64 (±0.16) (±standard deviation, PM1L) to 0.75 (±0.16) (PM2L), and the corresponding R^2 ranged from 0.61 (±0.16) to 0.65 (±0.17) (Figure 3). These suggest that the PM equation with a two-leaf upscaling strategy performed better than the MT equation.

3.3. Model-Data Agreement at Monthly and Seasonal Time Scales

[29] To explore the equations' responses to varying weather conditions during different seasons, we compared the simulated monthly and seasonal LE variations among the models for 20 sites in temperate and boreal zones (Table 4). Two tropical sites (ID-Pag and TH-Sak) were excluded, as ET shows hardly any seasonality under these climate conditions. The LE differences were not significant ($p > 0.05$) by one-way analysis of variance among three models during the same season but were significant during the different seasons for each model. For the four seasons, all three models underestimated LE in winter and spring seasons (negative bias), and three estimates were variable in summer and fall with both positive and negative biases. Removing biases of opposite sign, R values were close to 1.0 with large RMSE during the growing season for individual models. Moreover, model skill (Figure 4) and regression analysis (Table 4) show that PM2L performed well for summer (R = 0.81(±0.11)) and fall (R = 0.72 (±0.12)) across the 20 sites, while MT was better than PM2L for winter (R = 0.44 (±0.22)) and spring (R = 0.72 (±0.17)). Overall, all three models performed well in summer and less well during the other seasons, indicating that it may be challenging to capture ET dynamics during the cold season.

[30] Figure 5 compared simulations and observations of monthly composite diurnal variations. Examples are presented for each plant functional types. Overall modeled LE captured the observed diurnal variation within or near the margins of

Figure 3. Comparison of the observed daily averaged latent heat flux (LE) simulated by MT (open symbols, blue lines), PM1L (gray symbols, green lines), and PM2L (dark symbols, red lines) across the selected 22 sites for different plant functional types: (a,b) needleleaf evergreen forests in temperate and boreal zones; (c) needleleaf deciduous forest in boreal zone; (d,e) broadleaf evergreen forests in tropical and temperate zones; (f,g) broadleaf deciduous forests in temperate and boreal zones; (h,i) broadleaf deciduous shrubs in temperate and boreal zones; and (j) grasslands.

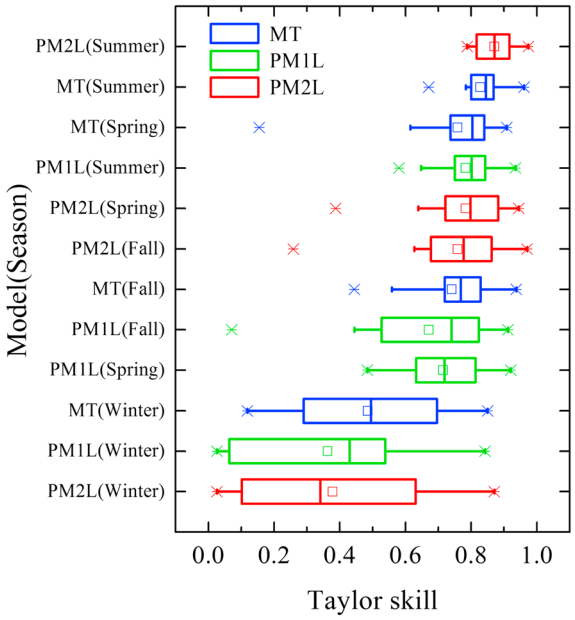

Figure 4. Boxplots of Taylor skill (*S*) for half-hourly *LE* by models and seasons across the selected 20 sites in temperate and boreal regions. Panels show interquartile range (box), mean (square), median (solid line), range (whiskers), and outliers (cross). Colors indicate models: blue for MT, green for PM1L, and red for PM2L. Models and seasons sorted by the median Taylor skill.

±1 standard deviation range of the mean observations for most site-years, except for the US-MOz site (Figure 5f), in which underestimation by all the three models occurred during the winter and early spring. The MT equation performance was variable in seasonal simulation, especially in summer (from June to August). For instance, for some boreal forest sites (FI-Hyy and DK-Sor), it underestimated *LE* by 30% on average (Figures 5c and 5g), while it overestimated *LE* by 91% on average for a tropical climate site (TH-Sak, Figure 5d) and two sites in mediterranean climate zones (FR-Pue and US-MOz, Figures 5e and 5f). *LE* modeled by the PM equations (PM1L and PM2L) was quite consistent with measurements without obvious bias for all the EC sites during the warm seasons. Linear regression analyses of the diurnal composites for these site-years showed that the values of R^2 were 0.57–0.95 and 0.60–0.96 for PM1L and PM2L, respectively, and the corresponding RMSE were 10.7–54.3 W m^{-2} and 6.9–50.6 W m^{-2}. Systematic biases as a result of using PM1L were found for most of the 10 sites with the one-leaf strategy generally underestimating *LE* around midday in the warm seasons (Figure 5).

3.4. Dominant Factors in ET Estimation Approaches

[31] To explore the further reasons that induced the differences among the ET estimations mentioned above, we conducted a set of sensitivity tests and assessed them as errors. Table 5 shows that the ET estimations varied within 12% of their base values when the parameters in each of these models increased or decreased by 20%.

[32] The relative differences change by 6% to 12% with the slope of conductance-to-photosynthesis relationship (*m*, equation S25) was found for all of the three models. This PFTs-dependent factor is a constant and affects stomatal conductance in canopy transpiration and evaporation simulations (equations 2 and 6) by adopting the Ball-Woodrow-Berry conductance model in both of the two land surface models [*Chen et al.*, 2007a; *Oleson et al.*, 2010]. LAI is another sensitive factor in ET estimation. Increasing or decreasing it by 20% altered ET by ~5% on average (Table 5), with the increase mainly in canopy transpiration (data not shown). In general, modifying other parameters in the land surface models, such as maximum rate of carboxylation ($Vc_{\max}$, equation S19) for net photosynthesis and then for g_s, albedo (α, equations S8–S11), and friction velocity (u_*, equation S2) for aerodynamic resistance of canopy, caused ET to change in the same direction for the three models. Moreover, our test (Table 5) shows that there was little sensitivity of ET to variation in the clumping index (Ω). It is noteworthy that an increase or decrease of albedo by 20% changed the relative differences between the base values and three models by −3.0 to 3.1% (Table 5), even though the albedo was considered in the MT equation indirectly by effecting r_s^{sun} and r_s^{sha} in equation 10. Given the direct beam albedo and diffuse albedo in MT, radiative transfer within vegetative canopies was calculated from the two-stream approximation [*Sellers*, 1985]. As a part of the solutions, the photosynthetically active radiation absorbed by the vegetation was used to estimate the light-limited rate of carboxylation by the Farquhar's photosynthesis model and then the stomatal resistances of the sunlit and shaded leaves (r_s^{sun} and r_s^{sha}) by the Ball-Woodrow-Berry conductance model. The values of r_s^{sun} and r_s^{sha} were used in equation 10 to estimate ET based on the MT equation [*Oleson et al.*, 2010].

[33] Furthermore, we quantified the simulated differences in annual ET for each modeling test by normalizing the PM2L results. As shown in Table 5, all of the 10 cases, including the increase and decrease of input variables or parameters by 20%, changed in the same direction for PM1L with a relative error of around −18%, but for MT, relative errors were quite variable with a relative span from −3.9% to 2.4%. These results suggest that changes in parameters or input variables within 20% of their initial values can reduce the difference between the results of using the MT and PM equations but not for that between the one-leaf and two-leaf upscaling strategies both using the PM equation.

4. Discussion

4.1. Effects of Model Structure on ET Estimates

[34] The differences of ET estimate between these two LSMs were not indirectly caused by their uncertainties, because the same methods were adopted in each model to computer key variables for ET calculation, and the comparisons did not show systematic errors for model ET-sensitive variables (Figures 1a, 1b, and 1e–1h), though CLM overestimated the canopy temperature during the daytime and underestimated the value at nighttime (Figures 1c and 1d) for each site-year. We also found that for some sites, e.g., CA-Ca1 (Figure 5a), the monthly averaged diurnal composites of *LE* modeled by the MT equation were close to the observations (Figure 5) or even better than that by the PM equation. One possible reason for this is that the errors stemmed from the biases in simulated leaf temperature would be compensated by parameters

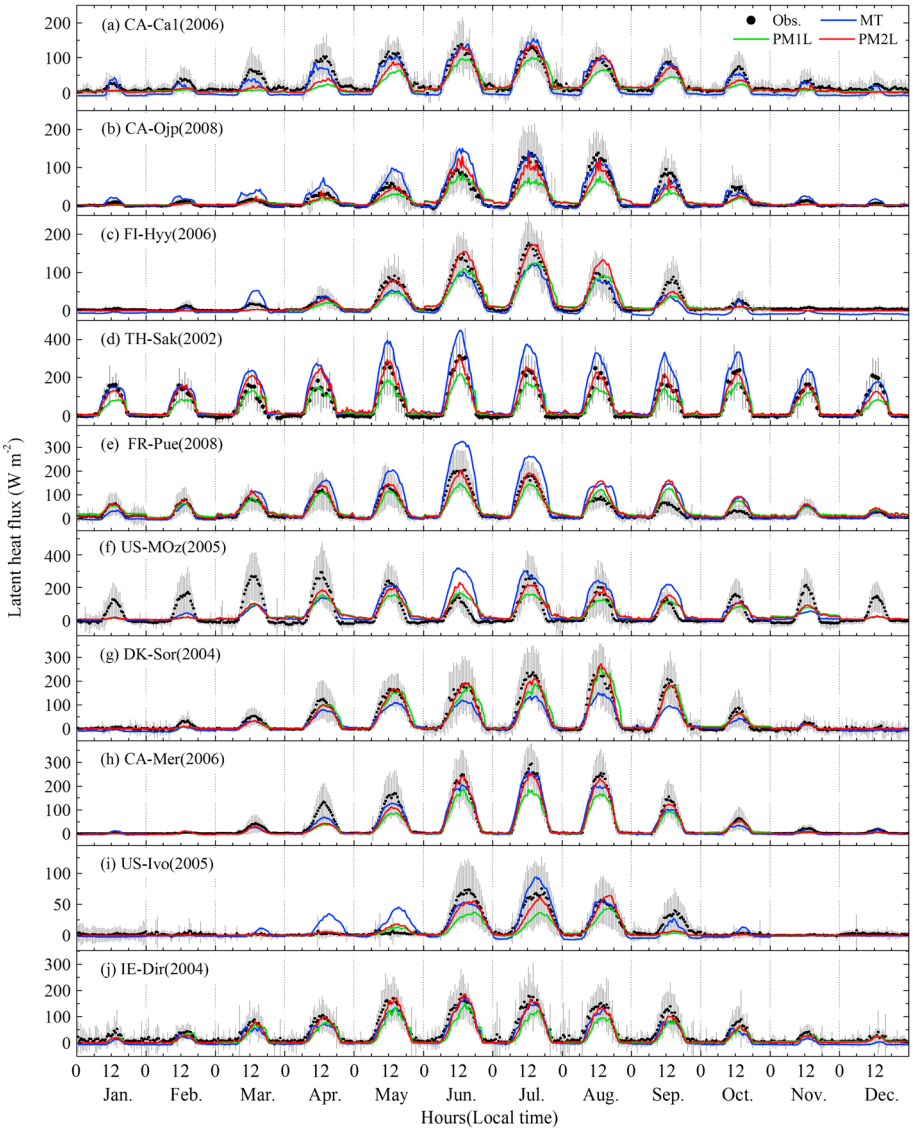

Figure 5. Monthly averaged diurnal composites of observed latent heat flux (dark lines) and simulated by MT (blue lines), PM1L (green lines), and PM2L (red lines) at sites representing each plant functional type: (a, b) needleleaf evergreen forests in temperate and boreal zones; (c) needleleaf deciduous forest in boreal zone; (d, e) broadleaf evergreen forests in tropical and temperate zones; (f, g) broadleaf deciduous forests in temperate and boreal zones; (h, i) broadleaf deciduous shrubs in temperate and boreal zones; and (j) grasslands. The gray bars indicate ±1 standard deviation of the averaged observations.

adjustment during the energy fluxes calculation. As described by *Bonan et al*. [2011] and *Chen et al*. [2010a], a revision of model parameters could reduce the errors caused by model structure and the improved carbon and energy fluxes estimation. A second possible cause is the structure of iterated process in modeling canopy energy fluxes. Based on these analyses, we believe that the errors in ET estimated by MT, PM1L, and PM2L are not mainly caused by the biases in the simulated ET-sensitive variables in CLM and DLM.

[35] There are two structural differences among the MT, PM1L, and PM2L models: (i) which upscaling strategy from leaf to canopy is adopted (i.e., one-leaf or two-leaf strategy) and (ii) whether the model separately calculate the net radiation at the interface between canopy and soil ($R_{n\hat{i}}$ in equitation 6). It is obvious that the variance in half-hourly and daily ET explained by the two-leaf strategy is better than that by the one-leaf strategy using the same PM equation (Figures 2, 3, and 5 and Tables 3 and 4). This is because the latter ignores a large contribution of diffuse PAR to the shaded leaves, which is more efficiently absorbed by the canopy for photosynthesis than direct PAR [*Dai et al*., 2004; *Sprintsin et al*., 2012]. Underestimation was also found in water vapor flux simulation by the MT equation with one-leaf strategy in CLM, but only for several PFTs (Figures 3a, 3c, and 3g). The other structural difference is the $R_{n\hat{i}}$. This variable is adopted by the PM equation (equation 6) but not employed by the MT equation (equations 3 and 4), which could explain the sensitivity difference of albedo between the two ET equations in Table 5. Using an improved model base on the PM equation to simulate soil evaporation and plant transpiration in a crop field, *Gao et al*. [2013] also found that the model was extremely sensitive to the radiation captured by crop. In

Table 5. Sensitivity of Site-Averaged Evapotranspiration (ET, mm H_2O yr^{-1}) to Errors in the Major Input Parameters of Leaf Area Index (LAI), Foliage Clumping Index (Ω), Slope of Conductance-to-Photosynthesis Relationship (m) for Stomatal Conductance, Maximum Rate of Carboxylation (Vc_{max}) for Photosynthesis, Albedo (α), and Friction Velocity (u_*) for Aerodynamic Resistance of Canopy

	MT	PM1L	PM2L	MT-Base	PM1L-Base	PM2L-Base	MT-PM2L	PM1L-PM2L
Base[a]	436.9(±284.7)[b]	354.1(±197.5)	435.6(±266.8)	—	—	—	1.3(0.3%)	−81.5(−18.7%)
1.2 × LAI	447.8(±333.3)	373.6(±215.8)	451.9(±280.8)	10.8(2.5%)[c]	19.5(5.5%)	16.3(3.7%)	−4.1(−0.9%)	−78.3(−17.3%)
0.8 × LAI	422.8(±316.4)	336.3(±193.4)	420.3(±267.3)	−14.1(−3.2%)	−17.8(−5.0%)	−15.4(−3.5%)	2.6(0.6%)	−84.0(−20.0%)
1.2 × Ω	—	354.8(±205.2)	436.0(±276.6)	—	0.7(0.2%)	0.4(0.1%)	—	−81.2(−18.6%)
0.8 × Ω	—	353.5(±201.4)	432.8(±268.5)	—	−0.6(−0.2%)	−2.8(−0.6%)	—	−79.3(−18.3%)
1.2 × m	479.6(±360.2)	376.9(±218.7)	468.4(±301.7)	42.7(9.8%)	22.7(6.4%)	32.8(7.5%)	11.2(2.4%)	−91.5(−19.5%)
0.8 × m	386.1(±277.3)	330.2(±182.9)	388.6(±235.0)	−50.9(−11.6%)	−23.9(−6.7%)	−47.0(−10.8%)	−2.5(−0.6%)	−58.4(−15.0%)
1.2 × Vc_{max}	438.2(±328.4)	369.7(±211.4)	456.0(±273.0)	1.3(0.3%)	15.6(4.4%)	20.3(4.7%)	−17.7(−3.9%)	−86.3(−18.9%)
0.8 × Vc_{max}	411.7(±306.8)	334.5(±190.2)	422.3(±260.2)	−25.3(−5.8%)	−19.7(−5.6%)	−13.3(−3.1%)	−10.7(−2.5%)	−87.9(−20.8%)
1.2 × α	432.6(±322.8)	344.9(±198.6)	422.6(±267.4)	−4.3(−1.0%)	−9.2(−2.6%)	−13.0(−3.0%)	10.0(2.4%)	−77.7(−18.4%)
0.8 × α	439.1(±327.0)	362.9(±206.5)	449.0(±280.3)	2.2(0.5%)	8.8(2.5%)	13.3(3.1%)	−9.8(−2.2%)	−86.1(−19.2%)
1.2 × u_*	446.1(±319.6)	358.3(±206.2)	442.3(±262.3)	9.1(2.1%)	4.2(1.2%)	6.7(1.5%)	3.8(0.8%)	−84.0(−19.0%)
0.8 × u_*	424.0(±315.0)	348.9(±197.5)	426.1(±264.0)	−13.0(−3.0%)	−5.2(−1.5%)	−9.5(−2.2%)	−2.1(−0.5%)	−77.2(−18.1%)

[a]The base values are calculated based on observed latent heat flux (LE) from eddy covariance tower measurements: ET = LE/λ. We assume a latent heat of vaporization (λ) of 2.501×10^6 J kg^{-1} [*Oleson et al*., 2010].
[b]Values in parentheses are standard deviations.
[c]The percentage in brackets is the difference relative to the base value.

the ET process, solar radiation proves the energy to change the state of the molecules of water on leaf/soil surface from liquid to vapor and control ET combined with the ambient temperate [*Allen et al*., 1998]. In general, increasing radiation loading on the leaf surface results in an increase in transpiration [*Phyo* and *Chung*, 2013], partly due to an increase in stomatal conductance [*Hetherington* and *Woodward*, 2003], and the difference between the rate of transpiration and the rate of production of water vapor inside the leaf by absorbed radiation controls the water potential of the epidermis in the leaf [*Pieruschka et al*., 2010]. Therefore, ignoring the impacts of solar radiation captured by leaf/soil will lead to errors in the estimates of water vapor fluxes. However, this could not be an important cause leading to the different performances between these two equations (MT and PM) in the two LSMs, because we did not find a systematic model bias in all the site-years simulations.

4.2. Seasonal Uncertainties in Model Performance

[36] The simulated ET with the MT equation has larger biases than with the PM equation (larger RMSE and σ_{norm}, Table 3 and Figure 2), especially for FI-Hyy, JP-Tom, FR-Pue and IT-Cpz. Table 6 shows that the daytime ET estimations by the MT equation during warm and wet seasons were almost equivalent to that during the whole year in IT-Cpz or even higher in FR-Pue, but the modeled values were 29% and 14% lower than the measurements in FI-Hyy and JP-Tom from May to October, respectively. A further exploration for the MT equation revealed that more water was lost as a result of canopy transpiration for these sites, which was ~10% high in warm and wet seasons compared with that in whole year around. It is similar to PM1L and PM2L, but the contribution of transpiration was ~6% high (Table 6). This result is consistent with our analysis results shown in Table 4. These ET estimation errors using the MT equation in CLM are expected to be stemmed from biases in calculations of transpiration, stomatal conductance, and photosynthesis (Table 5). The water vapor flux contributed from transpiration was relatively low during other seasons for all three models (Table 6).

[37] Many studies reported that the stomatal conductance and photosynthesis are changed with seasons or phenology. *Zhang et al*. [2009] estimated that the slope between net

Table 6. Total Evaportranspiration (ET, mm H_2O yr^{-1}) and Relative Contribution of Transpiration From Vegetation (T_C/ET) During the Daytime for the Whole Year and Seasons

			MT		PM1L		PM2L	
Number and Site ID	Year/Seasons	Observed ET	ET	T_C/ET	ET	T_C/ET	ET	T_C/ET
8 FI-Hyy	Whole year course	264.6[b]	189.9(−0.28)[c]	0.68	212.0(−0.20)	0.70	268.5(0.01)	0.71
	Warm and wet seasons[a]	239.1	170.3(−0.29)	0.74	202.9(−0.15)	0.72	255.8(0.07)	0.74
	Other seasons	25.5	19.6(−0.23)	0.15	9.1(−0.64)	0.18	12.7(−0.50)	0.20
9 JP-Tom	Whole year course	330.3	291.0(−0.12)	0.40	317.8(−0.04)	0.57	359.4(0.09)	0.54
	Warm and wet seasons	259.8	222.5(−0.14)	0.52	277.4(0.07)	0.64	285.5(0.10)	0.65
	Other seasons	70.5	68.5(−0.03)	0.01	40.4(−0.43)	0.07	73.9(0.05)	0.09
12 FR-Pue	Whole year course	399.0	621.7(0.56)	0.61	398.9(0.00)	0.48	408.0(0.02)	0.52
	Warm and wet seasons	271.9	473.9(0.74)	0.70	269.4(−0.01)	0.54	279.2(0.03)	0.58
	Other seasons	127.1	147.8(0.16)	0.34	129.5(0.02)	0.36	128.8(0.01)	0.39
13 IT-Cpz	Whole year course	317.5	510.3(0.61)	0.75	271.3(−0.15)	0.60	357.4(0.13)	0.64
	Warm and wet seasons	218.2	302.6(0.63)	0.85	185.2(−0.15)	0.66	247.2(0.13)	0.71
	Other seasons	99.3	207.7(1.09)	0.57	86.1(−0.13)	0.44	110.2(0.11)	0.46

[a]The warm and wet seasons involve summer and fall (from May to October). Two months are advanced for IT-Cpz because of its mediterranean climate.
[b]The value represents the water vapor flux with default parameters as shown in Table 5.
[c]The value in brackets is the difference relative to the observed ET.

assimilation rate (A_n) and stomatal conductance (g_s) for four broadleaf species significantly increased in the dry season compared with the wet season (Figure 4), indicating increased photosynthetic water-use efficiency. *Gratani et al*. [2000] also reported that the daily g_s/A_n change of a forest in the Mediterranean Basin could be described by a linear equation with negative slope over time (Figure 2), which was very close to 80 mol μmol^{-1} as the leaves expanded (February) but less than a half at midyear. Using a top-down approach based on a double-source canopy model and eddy flux measurements, *Ono et al*. [2013] estimated the canopy-scale relationship between gross photosynthesis adjusted for environmental variables and g_s for a paddy rice canopy throughout the growing season. They found that m appeared to vary seasonally with the ontogenic changes. Similarly, many studies have found that m could be higher in growth or young stages, e.g., in temperate deciduous broadleaf trees [*Kosugi et al*., 2003], tropical rainforest [*Kosugi et al*., 2012], boreal forest [*Stokes et al*., 2010], and grassland [*Wolf et al*., 2006], since there is a more rapid increase in g_s compared with the A_n during periods of leaf expansion [*England and Attiwill*, 2011; *Ono et al*., 2013]. However, two sensitive parameters m and Vc_{max} are empirical variables in the LSMs, which could not well capture temporal changes in g_s and A_n. Unrobustly, seasonal performance in ET simulation was also reported by *Schwalm et al*. [2010] by comparing monthly CO_2 exchange from 44 EC towers using 22 terrestrial biosphere models. It means that even these key parameters have been optimized well, the discrepancies between modeled seasonal photosynthesis and ET and observations could not be removed if the seasonal or phenology impacts are not reasonably considered by the models. Many efforts have been made to quantify the seasonal variations of some key parameters in g_s and A_n in calculation. In the parameterization in CLM4 for each ecoregion based on 3125 inventory plots measured during 2001 to 2006 in Oregon forests, *Hudiburg et al*. [2013] modeled monthly GPP that fell within the observed range of uncertainty for the majority of the year but still could not capture the seasonal response of Vc_{max} to temperature, precipitation, and day length. Moreover, the seasonal variation of Vc_{max} at the ecosystem scale was not sufficiently explained by upscaling with LAI [*Groenendijk et al*., 2011]. By changing the parameter m in the stomatal conductance calculation equation, *Zhu et al*. [2011] tested the observed responses of m to simulated net assimilation and transpiration rates. Their results suggest that more efforts are needed to adjust the values of some key parameters varying seasonally, such as m in land surface models in order to extend its application to regional or global scales. *Bonan et al*. [2011] and *Chen et al*. [2010a] pointed out that the uncertainties in land surface model estimations due to errors in input parameters would be the same as those from different structures. Our results agree with it, and we consider that the errors in modeling water vapor flux induced by the key parameters would be larger than those from the structures of ET equation.

[38] More than the model structures and variables, the uncertainties in seasonal ET estimates are also contributed from the EC data, which have gaps especially in the cold season. Even we have corrected energy fluxes according to the measured Bowen ratio (section 2.1). Following the linear regression slope from the ordinary least squares (OLSs) relationship between the half-hourly values of $LE + H$ against $R_n - G$ and energy balance ratio (EBR), i.e., $\Sigma(LE + H)/\Sigma(R_n - G)$, described by *Wilson et al*. [2002], we evaluated the energy balance closure of measurements over each season for 20 temperate and boreal sites. The results showed that the R^2 values of OLSs increased from winter to summer months, with an average of about 0.67 in January and February and 0.87 in July and August. The mean EBR is lower in winter (0.79) than in summer (0.84). It was associated with biophysical characteristics, where the sampling error is generally greater in open canopies or at topographically complex sites [*Misson et al*., 2007; *Scott et al*., 2004; *Scott*, 2010; *Stoy et al*., 2013; *Sun et al*., 2010]. Regarding the uncertainty resulting from spatial heterogeneity, an approach to deal with this issue is to couple a LSM with a footprint model, such as SAFE-f (Simple Analytical Footprint model on Eulerian coordinates for flux), in which the model considers the effects from land surface heterogeneity around the EC tower [*Chen et al*., 2009]. This method has been applied to assessing carbon budget estimation by combining EC flux and remote sensing at landscape to regional scales and to characterize the spatial representativeness of EC measurements [*Chen et al*., 2010b, 2011b]. However, its applications in land surface modeling are few. The combination of these two methods and the data-model fusion approach [*Chen et al*., 2010b; *Hu et al*., 2009; *Kattge et al*., 2009] would effectively increase the accuracy in upscaled regional flux estimation.

5. Conclusions

[39] By comparing the two commonly used equations for estimating terrestrial ET in land surface models across 10 PFTs across half-hourly, daily, monthly, and seasonal scales, our multisite study illustrated that the ET estimated by the MT equation in CLM has large uncertainties in warm and wet seasons, especially in deciduous forests. The errors mainly stemmed from ill parameterization in the stomatal conductance module. It raises a doubt on the accuracy of simulated temporal and spatial distribution of ET distribution by CLM even though the modeled global sum of water vapor flux was reasonable [*Bonan et al*., 2011; *Shi et al*., 2013]. Except for underestimation during cold season, the ET estimation by the PM equation is robust and much better with two-leaf strategy than with one-leaf strategy. This may attribute to its structure considering net radiation on both the surfaces of leaf and soil and the different contributions of diffused PAR to the shaded leaves compared to direct PAR to the sunlit leaves. This ET equations comparison study suggested the LSM community that the PM equation with a two-leaf canopy upscaling strategy is a better choice in ET simulation. One of future work directions is a need to improve seasonal or phenology variations of key parameters in stomatal conductance calculation to reduce the uncertainties in simulated ET in LSMs. Another thing worthy to do is to extend the calibration of the PM equation in DLM for cropland to expand its application to large heterogeneous of regions.

[40] **Acknowledgments.** This research was supported by a research grant (No. 2010CB950902 and 2010CB950904) under the Global Change Program of the Chinese Ministry of Science and Technology, a research grant (2012ZD010) of Key Project for the Strategic Science Plan in IGSNRR, CAS, a research grant funded by the China Postdoctoral Science Foundation (O7Z76032Z1), the research grants (41071059 and 41271116) funded by the National Science Foundation of China, a Research Plan of LREIS (O88RA900KA), CAS, and "One Hundred Talents" program funded by the Chinese Academy of Sciences. We acknowledge the agencies that supported the operations at the flux towers used here, which are part of FLUXNET. We

thank Mingliang Che for porting CESM, Xianming Dou for gap-filling meteorological data and two anonymous reviewers who provide useful comments that led to the improvement of this paper.

References

Allen, R. G., L. S. Pereira, D. Raes, and M. Smith (1998), Crop evapotranspiration: Guidelines for computing crop water requirements. *FAO Irrigation and Drainage Paper No. 56*. Rome, Italy: FAO.

Alton, P. B. (2011), How useful are plant functional types in global simulations of the carbon, water, and energy cycles?, *J. Geophys. Res.*, *116*, G01030, doi:10.1029/2010JG001430.

Alton, P. B., R. Ellis, S. O. Los, and P. R. North (2007), Improved global simulations of gross primary product based on a separate and explicit treatment of diffuse and direct sunlight, *J. Geophys. Res.*, *112*, D07203, doi:10.1029/2006JD008022.

Ball, J. T., I. E. Woodrow, and J. A. Berry (1987), A model predicting stomatal conductance and its contribution to the control of photosynthesis under different environmental conditions, in *Progress in Photosynthesis Research*, edited by J. Biggins, pp. 221–224, Martinus Nijhoff, Dordrecht, Netherlands.

Barr, A. G., et al. (2006), Climatic controls on the carbon and water balances of a boreal aspen forest, 1994–2003, *Global Change Biol.*, *12*, 1–16.

Bergeron, O., H. A. Margolis, T. A. Black, C. Coursolle, A. L. Dunn, A. G. Barr, and S. C. Wofsy (2007), Comparison of carbon dioxide fluxes over three boreal black spruce forests in Canada, *Global Change Biol.*, *13*, 89–107.

Blyth, E., J. Gash, A. Lloyd, M. Pryor, G. P. Weedon, and J. Shuttleworth (2010), Evaluating the JULES land surface model energy fluxes using FLUXNET data, *J. Hydrometeorol.*, *11*(2), 509–519.

Bonan, G. B. (2008), Forests and climate change: Forcings, feedbacks, and the climate benefits of forests, *Science*, *320*(5882), 1444–1449.

Bonan, G. B., K. W. Oleson, R. A. Fisher, G. Lasslop, and M. Reichstein (2012), Reconciling leaf physiological traits and canopy flux data: Use of the TRY and FLUXNET databases in the Community Land Model version 4, *J. Geophys. Res.*, *117*, G02026, doi:10.1029/2011JG001913.

Bonan, G. B., P. J. Lawrence, K. W. Oleson, S. Levis, M. Jung, M. Reichstein, D. M. Lawrence, and S. C. Swenson (2011), Improving canopy processes in the Community Land Model version 4 (CLM4) using global flux fields empirically inferred from FLUXNET data, *J. Geophys. Res.*, *116*, G02014, doi:10.1029/2010JG001593.

Cao, L., G. Balab, K. Caldeira, and R. Nemanid (2010), Importance of carbon dioxide physiological forcing to future climate change, *Proc. Natl. Acad. Sci. U.S.A.*, *107*(21), 9513–9518.

Chen, B., and N. C. Coops (2009), Understanding of coupled terrestrial carbon, nitrogen and water dynamics—An overview, *Sensors (Basel)*, *9*(11), 8624–8657.

Chen, B., N. C. Coops, T. A. Black, R. S. Jassal, J. M. Chen, and M. Johnson (2011a), Modeling to discern nitrogen fertilization impacts on carbon sequestration in a Pacific Northwest Douglas-fir forest in the first-postfertilization year, *Global Change Biol.*, *17*, 1442–1460.

Chen, B., et al. (2011b), Assessing eddy-covariance flux tower location bias across the Fluxnet-Canada Research Network based on remote sensing and footprint modelling, *Agric. For. Meteorol.*, *151*(1), 87–100.

Chen, B., J. M. Chen, and W. Ju (2007a), Remote sensing-based ecosystem–atmosphere simulation scheme (EASS)-model formulation and test with multiple-year data, *Ecol. Modell.*, *209*, 277–300.

Chen, B., J. M. Chen, G. Mo, C. W. Yuen, H. Margolis, K. Higuchi, and D. Chan (2007b), Modeling and scaling coupled energy, water, and carbon fluxes based on remote sensing: an application to Canada's landmass, *J. Hydrometeorol.*, *8*, 123–143.

Chen, B., Q. Ge, D. Fu, G. Yu, X. Sun, S. Wang, and H. Wang (2010b), A data-model fusion approach for upscaling gross ecosystem productivity to the landscape scale based on remote sensing and flux footprint modelling, *Biogeosciences*, *7*(9), 2943–2958.

Chen, B., T. A. Black, N. C. Coops, T. Hilker, J. A. Trofymow, and K. Morgenstern (2009), Assessing tower flux footprint climatology and scaling between remotely sensed and eddy covariance measurements, *Boundary Layer Meteorol.*, *130*(2), 137–167.

Chen, H., R. E. Dickinson, Y. Dai, and L. Zhou (2010a), Sensitivity of simulated terrestrial carbon assimilation and canopy transpiration to different stomatal conductance and carbon assimilation schemes, *Clim. Dyn.*, *36*, 1037–1054.

Chen, J. M., C. H. Menges, and S. G. Leblanc (2005b), Global mapping of foliage clumping index using multi-angular satellite data, *Remote Sens. Environ.*, *97*, 447–457.

Chen, J. M., G. Mo, J. Pisek, J. Liu, F. Deng, M. Ishizawa, and D. Chan (2012), Effects of foliage clumping on the estimation of global terrestrial gross primary productivity, *Global Biogeochem. Cycles*, *26*, GB1019, doi:10.1029/2010GB003996.

Chen, J. M., X. Chen, W. Ju, and X. Geng (2005a), Distributed hydrological model for mapping evapotranspiration using remote sensing inputs, *J. Hydrol.*, *305*, 15–39.

Collatz, G. J., J. T. Ball, C. Grivet, and J. A. Berry (1991), Physiological and environmental regulation of stomatal conductance, photosynthesis and transpiration: A model that includes a laminar boundary layer, *Agric. For. Meteorol.*, *51*, 109–136.

Cox, P. M., R. A. Betts, C. D. Jones, S. A. Spall, and I. J. Totterdell (2000), Acceleration of global warming due to carbon-cycle feedbacks in a coupled climate model, *Nature*, *408*, 184–187.

Dai, Y., R. E. Dickinson, and Y. Wang (2004), A Two-Big-Leaf model for canopy temperature, photosynthesis, and stomatal conductance, *J. Clim.*, *17*, 2281–2299.

Deng, F., J. M. Chen, S. Plummer, M. Chen, and J. Pisek (2006), Algorithm for global leaf area index retrieval using satellite imagery, *IEEE Trans. Geosci. Remote Sens.*, *44*(8), 2219–2229.

England, J. R., and P. M. Attiwill (2011), Changes in stomatal frequency, stomatal conductance and cuticle thickness during leaf expansion in the broad-leaved evergreen species, Eucalyptus regnans, *Trees*, *25*(6), 987–996.

Falge, E., et al. (2001), Gap filling strategies for defensible annual sums of net ecosystem exchange, *Agric. For. Meteorol.*, *107*, 43–69.

Farquhar, G. D., S. von Caemmerer, and J. A. Berry (1980), A biochemical model of photosynthetic CO_2 assimilation in leaves of C3 species, *Planta*, *149*, 78–90.

Fisher, J. B., T. A. DeBiase, Y. Qi, M. Xu, and A. H. Goldstein (2005), Evapotranspiration models compared on a Sierra Nevada forest ecosystem, *Environ. Modell. Software*, *20*(6), 783–796.

Flatau, P. J., R. L. Walko, and W. R. Cotton (1992), Polynomial fits to saturation vapor pressure, *J. Appl. Meteorol.*, *31*, 1507–1513.

Gao, Y., A. Duan, X. Qiu, X. Li, U. Pauline, J. Sun, and H. Wang (2013), Modeling evapotranspiration in maize/soybean strip intercropping system with the evaporation and radiation interception by neighboring species model, *Agric. Water Manage.*, *128*, 110–119.

Garbulksy, M. F., J. Peñuelas, D. Papale, and I. Fillela (2008), Remote estimation of carbon dioxide uptake by a Mediterranean forest, *Global Change Biol.*, *14*, 2860–2867.

Gent, P. R., et al. (2011), The Community Climate System Model Version 4, *J. Clim.*, *24*(19), 4973–4991.

Goulden, M. L., G. C. Winston, A. M. S. McMillan, M. E. Litvak, E. L. Read, A. V. Rocha, and J. R. Elliot (2006), An eddy covariance mesonet to measure the effect of forest age on land-atmosphere exchange, *Global Change Biol.*, *12*, 2146–2162.

Govind, A., J. M. Chen, H. Margolis, W. Ju, O. Sonnentag, and M. A. Giasson (2009), A spatially explicit hydro-ecological modeling framework (BEPS-TerrainLab V2.0): Model description and test in a boreal ecosystem in Eastern North America, *J. Hydrol.*, *367*(3–4), 200–216.

Grant, R. F., A. Arain, V. Arora, A. Barr, T. A. Black, J. Chen, S. Wang, F. Yuan, and Y. Zhang (2005), Intercomparison of techniques to model high temperature effects on CO2 and energy exchange in temperate and boreal coniferous forests, *Ecol. Modell.*, *188*(2–4), 217–252.

Grant, R. F., D. D. Baldocchi, and S. Ma (2012), Ecological controls on net ecosystem productivity of a seasonally dry annual grassland under current and future climates: Modelling with ecosys, *Agric. For. Meteorol.*, *152*, 189–200.

Gratani, L., P. Pesoli, M. F. Crescente, and K. Aichner (2000), Photosynthesis as a temperature indicator in Quercus ilex L, *Global Planet. Change*, *24*, 153–163.

Groenendijk, M., et al. (2011), Seasonal variation of photosynthetic model parameters and leaf area index from global Fluxnet eddy covariance data, *J. Geophys. Res.*, *116*, G04027, doi:10.1029/2011JG001742.

Grünwald, T., and C. Bernhofer (2007), A decade of carbon, water and energy flux measurements of an old spruce forest at the Anchor Station Tharandt, *Tellus B*, *59*, 387–396.

Gu, L. H., T. Meyers, S. G. Pallardy, P. J. Hanson, B. Yang, M. Heuer, K. P. Hosman, J. S. Riggs, D. Sluss, and S. D. Wullschleger (2006), Direct and indirect effects of atmospheric conditions and soil moisture on surface energy partitioning revealed by a prolonged drought at a temperate forest site, *J. Geophys. Res.*, *111*, D16102, doi:10.1029/2006JD007161.

Hetherington, A. M., and F. I. Woodward (2003), The role of stomata in sensing and driving environmental change, *Nature*, *424*, 901–908.

Hill, T. C., M. Williams, F. I. Woodward, and J. B. Moncrieff (2011), Constraining ecosystem processes from tower fluxes and atmospheric profile, *Ecol. Appl.*, *21*(5), 1474–1489.

Hirano, T., H. Segah, T. Harada, S. Limin, T. June, R. Hirata, and M. Osaki (2007), Carbon dioxide balance of a tropical peat swamp forest in Kalimantan, Indonesia, *Global Change Biol.*, *13*, 412–425.

Hirata, R., T. Hirano, N. Saigusa, Y. Fujinuma, K. Inukai, Y. Kitamori, Y. Takahashi, and S. Yamamoto (2007), Seasonal and interannual variations in carbon dioxide exchange of a temperate larch forest, *Agric. For. Meteorol.*, *147*, 110–124.

Hirata, R., et al. (2008), Spatial distribution of carbon balance in forest ecosystems across East Asia, *Agric. For. Meteorol.*, *148*(5), 761–775.

Hollinger, D. Y., et al. (2004), Spatial and temporal variability in forest atmosphere CO_2 exchange, *Global Change Biol.*, *10*, 1689–1706.

Hou, Z., M. Huang, L. R. Leung, G. Lin, and D. M. Ricciuto (2012), Sensitivity of surface flux simulations to hydrologic parameters based on an uncertainty quantification framework applied to the Community Land Model, *J. Geophys. Res.*, *117*, D15108, doi:10.1029/2012JD017521.

Hu, Z., et al. (2009), Partitioning of evapotranspiration and its controls in four grassland ecosystems: Application of a two-source model, *Agric. For. Meteorol.*, *149*(9), 1410–1420.

Hudiburg, T. W., B. E. Law, and P. E. Thornton (2013), Evaluation and improvement of the Community Land Model (CLM4) in Oregon forests, *Biogeosciences*, *10*(1), 453–470.

Ingwersen, J., et al. (2011), Comparison of Noah simulations with eddy covariance and soil water measurements at a winter wheat stand, *Agric. For. Meteorol.*, *151*(3), 345–355.

Jaksa, W. T., V. Sridhar, J. L. Huntington, and M. Khanal (2013), Evaluation of the complementary relationship using Noah Land Surface Model and North American Regional Reanalysis (NARR) data to estimate evapotranspiration in semiarid ecosystems, *J. Hydrometeorol.*, *14*(1), 345–359.

Jung, M., et al. (2010), Recent decline in the global land evapotranspiration trend due to limited moisture supply, *Nature*, *467*(7318), 951–954.

Kamo, K., T. Vacharangkura, S. Tiyanon, C. Viriyabuncha, S. Nimpila, and B. Doangsrisen (2002), Plant species diversity in tropical planted forests and implication for restoration of forest ecosystems in Sakaerat, Northeastern Thailand, *J. Agric. Res. Q.*, *36*(2), 111–118.

Kattge, J., W. Knorr, T. Raddatz, and C. Wirth (2009), Quantifying photosynthetic capacity and its relationship to leaf nitrogen content for global-scale terrestrial biosphere models, *Global Change Biol.*, *15*(4), 976–991.

Katul, G. G., R. Oren, S. Manzoni, C. Higgins, and M. B. Parlange (2012), Evapotranspiration: A process driving mass transport and energy exchange in the soil-plant-atmosphere-climate system, *Rev. Geophys.*, *50*, RG3002, doi:10.1029/2011RG000366.

Keenan, T. F., et al. (2012), Terrestrial biosphere model performance for inter-annual variability of land-atmosphere CO_2 exchange, *Global Change Biol.*, *18*(6), 1971–1987.

Kljun, N., T. A. Black, T. J. Griffis, A. G. Barr, D. Gaumont-Guay, K. Morgenstern, J. H. McCaughey, and Z. Nesic (2006), Response of net ecosystem productivity of three boreal forests stands to drought, *Ecosystems*, *9*, 1128–1144.

Kosugi, Y., S. Shibata, and S. Kobashi (2003), Parameterization of the CO_2 and H_2O gas exchange of several temperate deciduous broad-leaved trees at the leaf scale considering seasonal changes, *Plant, Cell Environ.*, *26*, 285–301.

Kosugi, Y., S. Takanashi, N. Yokoyama, E. Philip, and M. Kamakura (2012), Vertical variation in leaf gas exchange parameters for a Southeast Asian tropical rainforest in Peninsular Malaysia, *J. Plant Res.*, *125*(6), 735–748.

Krishnan, P., T. A. Black, N. J. Grant, A. G. Barr, E. H. Hogg, R. S. Jassal, and A. N. D. K. Morgenstern (2006), Impact of changing soil moisture distribution on net ecosystem productivity of a boreal aspen forest during and following drought, *Agric. For. Meteorol.*, *139*, 208–223.

Krishnan, P., T. A. Black, R. S. Jassal, B. Chen, and Z. Nesic (2009), Interannual variability of the carbon balance of three different-aged Douglas-fir stands in the Pacific Northwest, *J. Geophys. Res.*, *114*, G04011, doi:10.1029/2008JG000912.

Lafleur, P. M., N. T. Roulet, J. L. Bubier, S. Frolking, and T. R. Moore (2003), Interannual variability in the peatland-atmosphere carbon dioxide exchange at an ombrotrophic bog, *Global Biogeochem. Cycles*, *17*(2), 1036, doi:10.1029/2002GB001983.

Lawrence, D. M., et al. (2011), Parameterization improvements and functional and structural advances in version 4 of the Community Land Model, *J. Adv. Model Earth Syst.-Discuss.*, *3*, M03001, doi:10.1029/02011MS000045.

Lawrence, D. M., P. E. Thornton, K. W. Oleson, and G. B. Bonan (2007), The partitioning of evapotranspiration into transpiration, soil evaporation, and canopy evaporation in a GCM: Impacts on land–atmosphere interaction, *J. Hydrometeorol.*, *8*(4), 862–880.

Li, X. R., Q. Z. Liu, Z. Cai and Z. Q. Ma (2007) Specific leaf area and leaf area index of conifer plantations in Qianyanzhou station of subtropical China. *J. Plant Ecol.*, *31*(1), 93–101 (in Chinese with English abstract).

Marlin, B. (2004), Modeling user rating profiles for collaborative filtering, in *Advances in Neural Information Processing Systems*, vol. l6, pp. 627–634, MIT Press, Cambridge.

McMillan, A. M. S., G. C. Winston, and M. L. Goulden (2008), Age-dependent response of boreal forest to temperature and rainfall variability, *Global Change Biol.*, *14*(8), 1904–1916.

Mercado, L. M., C. Huntingford, J. H. C. Gash, P. M. Cox, and V. Jogireddy (2007), Improving the representation of radiation interception and photosynthesis for climate model applications, *Tellus B*, *59*(3), 553–565.

Misson, L., et al. (2007), Partitioning forest carbon fluxes with overstory and understory eddy-covariance measurements: A synthesis based on FLUXNET data, *Agric. For. Meteorol.*, *144*(1–2), 14–31.

Mo, X., J. M. Chen, W. Ju, and T. A. Black (2008), Optimization of ecosystem model parameters through assimilating eddy covariance flux data with an ensemble Kalman filter, *Ecol. Modell.*, *217*, 157–173.

Moffat, A. M., et al. (2007), Comprehensive comparison of gap-filling techniques for eddy covariance net carbon fluxes, *Agric. For. Meteorol.*, *147*(3–4), 209–232.

Montaldo, N., J. D. Albertson, and M. Mancini (2007), Dynamic calibration with an Ensemble Kalman Filter based data assimilation approach for root-zone moisture predictions, *J. Hydrometeorol.*, *8*(4), 910–921.

Monteith, J. (1965), Evaporation and environment, in *The State and Movement of Water in Living Organisms, 19th Symposium of the Society for Experimental Biology*, edited by G. E. Fogg, pp. 205–234, Cambridge Univ. Press, London.

Nazeer, M. (2010), Comparison of different methods for estimation of potential evapotranspiration, *The Nucleus*, *47*(1), 41–46.

Oechel, W. C., G. L. Vourlitis, S. J. Hastings, R. C. Zulueta, L. Hinzman, and D. Kane (2000), Acclimation of ecosystem CO_2 exchange in the Alaskan Arctic in response to decadal climate warming, *Nature*, *406*, 978–981.

Oki, T., and S. Kanae (2006), Global hydrological cycles and world water resources, *Science*, *313*(5790), 1068–1072.

Oleson, K. W., et al. (2010), *Technical description of version 4.0 of the Community Land Model (CLM)*, National Center for Atmospheric Research, Boulder, Colorado.

Ono, K., A. Maruyama, T. Kuwagata, M. Mano, T. Takimoto, K. Hayashi, T. Hasegawa, and A. Miyata (2013), Canopy-scale relationships between stomatal conductance and photosynthesis in irrigated rice, *Global Change Biol.*, *19*(7), 2209–2220, doi:10.1111/gcb.12188.

Peichl, M., P. Leahy, and G. Kiely (2011), Six-year stable annual uptake of carbon dioxide in intensively managed humid temperate grassland, *Ecosystems*, *14*, 112–126.

Phyo, A. K., and N. J. Chung (2013), Response of single leaf photosynthesis and transpiration to red light and UV-A radiation in two different plant-type rice cultivars (*Oryza sativa* L.), *Australian J. Crop Sci.*, *7*(1), 119–129.

Pieruschka, R., G. Huber, and J. A. Berry (2010), Control of transpiration by radiation, *Proc. Natl. Acad. Sci. U.S.A.*, *107*, 13,372–13,377.

Pilegaard, K., T. N. Mikkelsen, C. Beier, N. O. Jensen, P. Ambus, and H. Ro-Poulsen (2003), Field measurements of atmosphere-biosphere interactions in a Danish beech forest, *Boreal Environ. Res.*, *8*, 315–333.

Qian, T., A. Dai, K. E. Trenberth, and K. W. Oleson (2006), Simulation of global land surface conditions from 1948 to 2004. Part I: Forcing data and evaluations, *J. Hydrometeorol.*, *7*, 953–975.

Rambal, S., J. M. Ourcival, R. Joffre, F. Mouillot, Y. Nouvellon, M. Reichstein, and A. Rocheteau (2003), Drought controls over conductance and assimilation of a Mediterranean evergreen ecosystem: Scaling from leaf to canopy, *Global Change Biol.*, *9*, 1813–1824.

Reichstein, M., et al. (2007), Reduction of ecosystem productivity and respiration during the European summer 2003 climate anomaly: A joint flux tower, remote sensing and modelling analysis, *Global Change Biol.*, *13*(3), 634–651.

Roulet, N. T., P. M. Lafleur, P. J. H. Richard, T. R. Moore, E. R. Humphreys, and J. Bubier (2007), Contemporary carbon balance and late Holocene carbon accumulation in a northern peatland, *Global Change Biol.*, *13*, 397–411.

Schaefer, K., et al. (2012), A model-data comparison of gross primary productivity: Results from the North American Carbon Program site synthesis, *J. Geophys. Res.*, *117*, G03010, doi:10.1029/2012JG001960.

Schwalm, C. R., et al. (2010), A model-data intercomparison of CO_2 exchange across North America: Results from the North American Carbon Program site synthesis, *J. Geophys. Res.*, *115*, G00H05, doi:10.1029/2009jg001229.

Scott, R. L. (2010), Using watershed water balance to evaluate the accuracy of eddy covariance evaporation measurements for three semiarid ecosystems, *Agric. For. Meteorol.*, *150*(2), 219–225.

Scott, R. L., E. A. Edwards, W. J. Shuttleworth, T. E. Huxman, C. Watts, and D. C. Goodrich (2004), Interannual and seasonal variation in fluxes of water and carbon dioxide from a riparian woodland ecosystem, *Agric. For. Meteorol.*, *122*(1–2), 65–84.

Sellers, P. J. (1985), Canopy reflectance, photosynthesis and transpiration, *Int. J. Remote Sens.*, *6*(8), 1335–1372.

Sentelhas, P. C., T. J. Gillespie, and E. A. Santos (2010), Evaluation of FAO Penman–Monteith and alternative methods for estimating reference evapotranspiration with missing data in Southern Ontario, Canada, *Agric. Water Manage.*, *97*(5), 635–644.

Shi, X., J. Mao, P. E. Thornton, and M. Huang (2013), Spatiotemporal patterns of evapotranspiration in response to multiple environmental factors simulated by the Community Land Model. *Environ. Res. Lett.*, *8*, 024012, 1–12.

Shuttleworth, W. J., and J. S. Wallace (1985), Evaporation from sparse crops-an energy combination theory, *Q. J. R. Meteorol. Soc.*, *111*, 839–855.

Singh, V. P., and C. Y. Xu (1997), Evaluation and generalization of 13 mass-transfer equations for determining free water evaporation, *Hydrol. Processes*, *11*, 311–323.

Sprintsin, M., J. M. Chen, A. Desai, and C. M. Gough (2012), Evaluation of leaf-to-canopy upscaling methodologies against carbon flux data in North America, *J. Geophys. Res.*, *117*, G01023, doi:10.1029/2010JG001407.

Stannard, D. I. (1993), Comparison of Penman-Monteith, Shuttleworth-Wallace, and Modified Priestley-Taylor evapotranspiration models for wild land vegetation in semiarid rangeland, *Water Resourc.Res.*, *29*(5), 1379–1392.

Stöckli, R., D. M. Lawrence, G. Y. Niu, K. W. Oleson, P. E. Thornton, Z. L. Yang, G. B. Bonan, A. S. Denning, and S. W. Running (2008), Use of FLUXNET in the Community Land Model development, *J. Geophys. Res.*, *113*, G01025, doi:10.1029/2007JG000562.

Stokes, V. J., M. D. Morecroft, and J. I. L. Morison (2010), Comparison of leaf water use efficiency of oak and sycamore in the canopy over two growing seasons, *Trees*, *24*(2), 297–306.

Stoy, P. C., et al. (2013), A data-driven analysis of energy balance closure across FLUXNET research sites: The role of landscape scale heterogeneity, *Agric. Water Manage.*, *171–172*, 137–152.

Subin, Z. M., W. J. Riley, J. Jin, D. S. Christianson, M. S. Torn, and L. M. Kueppers (2011), Ecosystem feedbacks to climate change in California: Development, testing, and analysis using a coupled regional atmosphere and land surface model (WRF3–MT3.5), *Earth Interact.*, *15*(15), 1–38.

Sun, G., A. Noormets, M. J. Gavazzi, S. G. McNulty, J. Chen, J. C. Domec, J. S. King, D. M. Amatya, and R. W. Skaggs (2010), Energy and water balance of two contrasting loblolly pine plantations on the lower coastal plain of North Carolina, USA, *For. Ecol. Manage.*, *259*(7), 1299–1310.

Tabari, H., S. Trajkovic, and M. E. Grismer (2011), Comparative analysis of 31 reference evapotranspiration methods under humid conditions, *Irrig. Sci.*, *31*(2), 107–117.

Tang, S., J. M. Chen, Q. Zhu, X. Li, M. Chen, R. Sun, Y. Zhou, F. Deng, and D. Xie (2007), An LAI inversion algorithm based on directional reflectance kernels, *J. Environ. Manage.*, *85*, 638–648.

Tanja, S., et al. (2003), Air temperature triggers the recovery of evergreen boreal forest photosynthesis in spring, *Global Change Biol.*, *9*, 1410–1426.

Taylor, K. E. (2001), Summarizing multiple aspects of model performance in a single diagram, *J. Geophys. Res.*, *106*(D7), 7183–7192.

Twine, T. E., W. P. Kustas, J. M. Norman, D. R. Cook, P. R. Houser, T. P. Meyers, J. H. Prueger, P. J. Starks, and M. L. Wesely (2000), Correcting eddy-covariance flux underestimates over a grassland, *Agric. Water Manage.*, *103*, 279–300.

Valentini, R., P. D. Angelis, G. Matteuci, R. Monaco, S. Dore, and G. E. Scarascia Mucnozza (1996), Seasonal net carbon dioxide exchange of a beech forest with the atmosphere, *Global Change Biol.*, *2*, 199–207.

Verseghy, D. L., N. A. McFarlane, and M. Lazare (1993), CLASS-A Canadian land surface scheme for GCMS, II vegetation model and coupled runs, *Int. J. Climatol.*, *13*, 347–370.

Verstraeten, W. W., F. Veroustraete, and J. Feyen (2008), Assessment of evapotranspiration and soil moisture content across different scales of observation, *Sensors*, *8*, 70–117.

Vinukollu, R. K., J. Sheffield, E. F. Wood, M. G. Bosilovich, and D. Mocko (2012), Multi-model analysis of energy and water fluxes: Intercomparisons between operational analyses, a land surface model, and remote sensing, *J. Hydrometeorol.*, *13*(1), 3–26.

Vinukollu, R. K., R. Meynadier, J. Sheffield, and E. F. Wood (2011), Multi-model, multi-sensor estimates of global evapotranspiration: Climatology, uncertainties and trends, *Hydrol. Processes*, *25*(26), 3993–4010.

Vörösmarty, C. J., C. J. Willmott, B. J. Choudhury, A. L. Schloss, T. K. Stearns, S. M. Robeson, and T. J. Dorman (1996), Analyzing the discharge regime of a large tropical river through remote sensing, ground-based climatic data, and modeling, *Water Resour. Res.*, *32*(10), 3137–3150.

Wang, Z., et al. (2011), Evaluating weather effects on interannual variation in net ecosystem productivity of a coastal temperate forest landscape: A model intercomparison, *Ecol. Modell.*, *222*(17), 3236–3249.

Willmott, C. J. (1982), Some comments on the evaluation of model performance, *Bull. Am. Meteorol. Soc.*, *63*(11), 1309–1313.

Willmott, C. J., and K. Matsuura (2005), Advantages of the mean absolute error (MAE) over the root mean square error (RMSE) in assessing average model performance, *Climate Res.*, *30*, 79–82.

Willmott, C. J., S. G. Ackleson, R. E. Davis, J. J. Feddema, K. M. Klink, D. R. Legates, J. O'Donnell, and C. M. Rowe (1985), Statistics for the evaluation and comparison of models, *J. Geophys. Res.*, *90*(C5), 8995–9005.

Wilson, K. B., et al. (2002), Energy balance closure at FLUXNET sites, *Agric. For. Meteorol.*, *113*, 223–243.

Wohlfahrt, G., A. Hammerle, A. Haslwanter, M. Bahn, U. Tappeiner, and A. Cernusca (2008), Seasonal and inter-annual variability of the net ecosystem CO_2 exchange of a temperate mountain grassland: Effects of weather and management, *J. Geophys. Res.*, *113*, D08110, doi:10.1029/2007JD009286.

Wolf, A., K. Akshalov, N. Saliendra, D. A. Johnson, and E. A. Laca (2006), Inverse estimation of Vcmax, leaf area index, and the Ball-Berry parameter from carbon and energy fluxes, *J. Geophys. Res.*, *111*, D08S08, doi:10.1029/2005JD005927.

Zhang, J. L., L. Z. Meng, and K. F. Cao (2009), Sustained diurnal photosynthetic depression in uppermost-canopy leaves of four dipterocarp species in the rainy and dry seasons: Does photorespiration play a role in photoprotection?, *Tree Physiol.*, *29*(2), 217–228.

Zhu, G. F., X. Li, Y. H. Su, L. Lu, and C. L. Huang (2011), Seasonal fluctuations and temperature dependence in photosynthetic parameters and stomatal conductance at the leaf scale of *Populus euphratica* Oliv, *Tree Physiol.*, *31*, 178–195.